AN EXPERIMENTAL INVESTIGATION OF NONEQUILIBRIUM PHYSICS AND DYNAMICAL SYSTEMS IN TURBULENT FLUIDS.

by

Mahesh M. Bandi

B. E. Computer Science & Engineering, University of Madras, 1998.

M. S. Electrical Engineering, University of Pittsburgh, 2002.

M. S. Physics, University of Pittsburgh, 2004.

Submitted to the Graduate Faculty of

the Department of Physics and Astronomy in partial fulfillment

of the requirements for the degree of

Doctor of Philosophy

University of Pittsburgh

2006

UNIVERSITY OF PITTSBURGH

DEPARTMENT OF PHYSICS AND ASTRONOMY

This dissertation was presented

by

Mahesh M. Bandi

It was defended on

July 14, 2006

and approved by

W. I. Goldburg, Professor Emeritus, Department of Physics & Astronomy

D. Boyanovsky, Professor, Department of Physics & Astronomy

Y. Y. Goldschmidt, Professor, Department of Physics & Astronomy

X.-L. Wu, Professor, Department of Physics & Astronomy

J. Boudreau, Professor, Department of Physics & Astronomy

B. Ermentrout, Professor, Mathematics Department

Dissertation Director: W. I. Goldburg, Professor Emeritus, Department of Physics & Astronomy

AN EXPERIMENTAL INVESTIGATION OF NONEQUILIBRIUM PHYSICS AND DYNAMICAL SYSTEMS IN TURBULENT FLUIDS.

Mahesh M. Bandi, PhD

University of Pittsburgh, 2006

Experiment 1 studies finite system size effects on temporal energy flux fluctuations in three-dimensional (3D) incompressible turbulence. The measured instantaneous energy flux shows that the turbulent energy transfer proceeds towards small spatial scales on average but frequently reverses direction (backscatter) to travel towards larger scales. The frequency of backscatter events is studied experimentally and through simulations.

In Experiment 2 the third-order Eulerian structure function is measured for compressible turbulence on a free surface for the first time, and is found to scale linearly in space and agrees well with Kolmogorov's theory of 1941 (K41). K41 predicts the second-order Lagrangian structure function should scale linearly in time. However the experimental measurements show it instead scales as a power-law with exponent 1/2.

Experiment 3 concerns measurement of entropy production rate in steady-state compressible turbulence. The analysis relies on the recent theory of Falkovich and Fouxon. The entropy rate is expected to equal the time integral of the lagrangian velocity divergence correlation function with a negative prefactor. The experimental results are found to disagree with this prediction. In addition, if the system is highly chaotic (follows SRB statistics), the system's entropy rate equals the sum of its Lyapunov exponents. The measured entropy rate agrees well with the sum of Lyapunov exponents obtained from simulations by Boffetta et. al. under flow conditions similar to the experiment.

Experiment 4 presents a test of the Steady-State Fluctuation Theorem of Gallavotti and Cohen for entropy rate statistics collected from the individual lagrangian trajectories

of experiment 3. The entropy rate statistics show excellent agreement with the Fluctuation Theorem within a limited interval of the probability distributions and limited window of averaging times.

Keywords: Fluid Turbulence, Nonlinear Dynamics, Dynamical Systems, Nonequilibrium Physics, Statistical Mechanics.

TABLE OF CONTENTS

LIST OF TABLES

LIST OF FIGURES

PREFACE

This document was made possible by the kind support of many people. The faculty and staff of the department of Physics and Astronomy have helped in many ways during my four year stay here. I thank them all for their help.

Rob Cressman was instrumental in introducing me to Walter and his wonderful lab. Despite his busy postdoctoral schedule, he has always found time to discuss research and help me with ideas to tackle or implement problems. Beyond research he has also helped me deal with the more difficult aspects of graduate life. I found a fine friend in him, and will work hard to maintain it in future too.

My time in the lab was made comfortable by my fellow students in the Softmatter group, I thank them all and wish them the best in all their future endeavours, both professional and personal.

Xiao-lun merits a special mention for he has always mentored me in the background, probably without realizing it. He was my sounding board on many half-baked ideas. His unflinching commitment and self-critical approach to work in general, and physics in particular were a constant source of encouragement to me. He will always have my deepest respect.

I thank members of my dissertation committee, Professors Goldschmidt, Boudreau, Boyanovsky, Ermentrout, Xiao-lun and Walter for guiding my thesis work.

My limited understanding of Dynamical Systems in general, and the turbulence problem in specific would not be possible if not for the wise counsel of kind people scattered across the world who work hard and ponder over these problems deeply. I acknowledge help from Itamar Procaccia, Grisha Falkovich and Elisha Moses (Weizmann Institute of Science, Israel), Misha Chertkov, Colm Connaughton, Susan Kurien, Mike Rivera and Bob Ecke (CNLS, Los Alamos), Knut Jorgen Maloy (Oslo, Norway), Guido Boffetta (Torino, Italy), Eberhard

Bodenschatz (Göttingen, Germany), Zellman Warhaft (Cornell), Sara Majetich (Carnegie Mellon), Elisabeth Bouchaud (CEA Saclay, France), Jean-Francois Pinton and Krzysztof Gawedzki (ENS-Lyon, France), Jörg Schumacher (Ilmenau, Germany), Bruno Eckhardt and Jahanshah Davoudi (Marburg, Germany), Katepalli Sreenivasan (ICTP Trieste, Italy), Dan Lathrop and Ed Ott (Maryland), Jerry Gollub and Sebastian Aumaitre (Haverford College), Yuan-Nan Young (NJIT), Jun Zhang, Mike Shelley and Steve Childress (Courant Institute of Mathematical Sciences, NYU), Christos Vassilicos (Imperial College, London), Charles Meneveau, Laurent Chevillard, and Gregory Eyink (Johns Hopkins), Giovanni Gallavotti (INFN, Rome), Nigel Goldenfeld, Gustavo Gioia and Alfred Hubler (UIUC, Urbana), Wendy Zhang (UChicago), Penger Tong (Hong Kong), Hamid Kellay (Bordeaux, France), Douglas Durian, Andrea Liu, Klebert Feitosa and Paolo Arratia (UPenn, Philadelphia), Detlef Lohse (UTwente, Sweden), Willem van de Water (Eindhoven, Netherlands). Many of them were very kind to help me with ideas and suggestions, some invited me to their home institutions and indulged me in stimulating conversations on physics, and a few have honored me with co-authorship on my publications. Lastly I acknowledge Alain Pumir at Institute Non Lineaire de Nice, CNRS and Universite de Nice. He is a friend, mentor, and an amazing person to collaborate with. Parts of this thesis came from his work. I hope to have many more opportunities in future to work with him again.

My acknowledgements are incomplete without mentioning my family and my mentor. My parents toiled hard to see their sons become good citizens. They made many sacrifices to ensure we had the opportunities they were denied. I am painfully aware of some, many others I do not even know of. I can only hope their efforts have not gone in waste. Likewise, Walter picked me up at a time when almost everyone, including myself, had little hopes of my survival in graduate school. He taught me most of the Physics I know today, sometimes late into the night at the blackboard. He was delighted to watch things go my way and suffered with me when I was in pain. I consider myself most fortunate to have found him for a *Guru*, there could have been none other. The document is naturally dedicated to my parents and to Walter, my intellectual father.

"It is understood by him, by whom it is not understood,
and the one who understands it, knows it not."

- Kena Upanishad.

"It is conceived by him, by whom it is not conceived,
and the one who conceived it, knows it not."

- Lao Tzu.

1.0 INTRODUCTION.

1.1 INTRODUCTION.

The turbulence problem is normally considered the oldest unsolved problem in classical physics. The absence of a satisfactory explanation is certainly not due to lack of interest or effort. In the author's opinion, the primary obstacle to approaching this nonequilibrium phenomenon lies within the multiple spatial and temporal scales at which the turbulence process operates (at least within the context of incompressible turbulence). Considered by some as "the graveyard of theories" [61], this problem has attracted attention from some of the most brilliant minds in physics that include W. Heisenberg [36], L. Onsager [24], L. D. Landau [40], A. N. Kolmogorov [38, 29], G. I. Taylor [69, 70], G. K. Batchelor [6] among many more. Many have tried to reign in the fantastically many degrees of freedom involved in the study of turbulent fluids, but the problem may have more surprises curled up its sleeve than it has revealed yet.

At present, there exist two established approaches to studying turbulence. Traditionally, turbulence has been studied as a nonequilibrium hydrodynamic process within the framework of fluid dynamics where the Navier-Stokes equation forms the starting point. The second and more recent approach recognizes the turbulence mechanism as an instance of chaos in fluids. Both approaches have their own merits and each has led to new insights [29, 62] allowing an improved understanding of turbulence. The experiments detailed in this dissertation study turbulence within both contexts. They also study two specific situations in turbulence, incompressible turbulence for which a rich theory is already available, and compressible turbulence at a free surface for which currently no theory exists.

1.1.1 TURBULENCE IN THE HYDRODYNAMIC CONTEXT.

The turbulence problem has historically been treated within the framework of fluid dynamics leading to a rich theory that finds its basis in the Navier-Stokes Equation (Eq. 1.1) (it is usually studied in the incompressible regime where the divergence of turbulent velocity field is identically zero everywhere within the fluid (see Eq. 1.2)).

$$\frac{\partial \mathbf{v}}{\partial t} + (\mathbf{v} \cdot \vec{\nabla})\mathbf{v} = -\frac{\vec{\nabla} p}{\rho} + \nu \nabla^2 \mathbf{v} \tag{1.1}$$

where $\mathbf{v}$ is the velocity field, p is the pressure, ρ is the fluid density and ν is the kinematic viscosity and is related to the fluid viscosity η through the relation $\nu = \eta/\rho$.

$$\vec{\nabla} \cdot \mathbf{v} = 0 \tag{1.2}$$

The finest hour of this approach most certainly arrived with Kolmogorov's celebrated phenomenological theory of 1941 (K41) [38], where he derived an exact and non-trivial result for incompressible turbulence within a statistical fluid dynamics context. This result now known as the four-fifth law relates the third-order structure function of longitudinal velocity differences $S_3(r) \equiv \langle (\Delta u_L(r))^3 \rangle$ (an experimentally measured quantity) at a given spatial scale to the mean rate of energy transfer through the turbulent fluid at that particular scale ($S_3(r) = -(4/5)\bar{\varepsilon} r$, here $\bar{\varepsilon}$ is the mean energy flux and r is the spatial scale in question) . The result is applicable to isotropic, incompressible, and homogeneous turbulence within a range of spatial scales collectively referred to as the inertial range of turbulence. K41 forms the basis for most studies in modern turbulence research today.

Kolmogorov extended the four-fifth law using dimensional arguments and predicted that higher n^{th} order structure functions would scale as $S_n(r) \equiv \langle (\Delta u_L(r))^n \rangle \sim (\bar{\varepsilon} r)^{n/3}$. This prediction, called the self-similarity hypothesis is now known to fail due to disagreement between Kolmogorov's prediction and experimentally observed scaling. This mismatch has come to be known as the anomalous or multi-scaling problem in incompressible turbulence, and is attributed to extremely wild velocity fluctuations (intermittency) [2, 8, 45] in turbulent flows. There has been much effort to understand the source of intermittency and to reconcile it with the anomalous scaling problem, thus spawning a multitude of models. A

detailed explanation of intermittency and various models associated with it is available in [29] (for more recent methods since 1995, see [27, 42]). Recent evidence also shows anomalous scaling exponents may be retrieved from a linear model derived from a nonlinear model [1], suggesting that scaling anomalies may have nothing to do with nonlinearities in turbulence. Despite the great import of the intermittency problem, it does not form the primary focus of experiments discussed here. However intermittency effects do form a part of the interpretation of experimental results, hence the digression to provide this short background.

1.1.2 TURBULENCE AS A CHAOTIC DYNAMICAL SYSTEM.

Unlike the hydrodynamic approach, the study of turbulence as a chaotic dynamical process started with a specific result. The transition of fluid flow from laminar to turbulent regime has been a subject of intense study for a long time. Osborne Reynolds [57] recognized coherent travelling waves prior to the onset of turbulence in pipe flows as early as 1883. Much of the interest was generated by the importance of turbulence in pipe flows in engineering applications [52]. Landau [40] proposed that the physical parameters x describing a fluid in turbulent motion were quasi-periodic functions in time:

$$x(t) = f(\omega_1 t, ..., \omega_i t) \tag{1.3}$$

where f has period 1 separately for each argument and the frequencies $\omega_1, ..., \omega_i$ are not rationally related, leading to the expectation that i becomes large for large Reynolds numbers leading to complicated and irregular behavior characteristic of turbulent motion in fluids.

Landau's proposal leads to the interpretation that the turbulent state of a fluid results from a large number of discrete transitions or bifurcations, each of which causes the velocity field to oscillate with a different frequency ω_i. As the Reynolds number of the system increases so do the bifurcations leading to a steady increase in i, the number of oscillatory modes. At a sufficiently large Reynolds number (or equivalently large i), the motion appears chaotic. This feature can be experimentally captured by the fact that the temporal correlation function of the velocity field $C(\tau) = \frac{\langle v(t)v(t+\tau)\rangle}{\langle v^2\rangle}$ (the angular brackets here would denote an average over time t) does not strictly go to zero as $\tau \to \infty$. In a nutshell Landau's

argument implies the transition from laminar to turbulent flow proceeds continuously.

Ruelle and Takens [63] instead applied the then nascent theory of dynamical systems and argued that the transition to turbulence should be sudden, aperiodic, and the transition itself should arise after a short number of bifurcations with exponentially damped correlations (ie. $C(\tau)$ would decay to zero in finite τ). In an experiment conducted in Taylor-Couette flow, Gollub and Swinney [34] provided conclusive proof in favour of the Ruelle-Takens proposal in 1975. Around the same time numerical simulations in Rayleigh-Bénard convection [44] also found a sharp transition to chaotic regime in accord with the Ruelle-Takens picture. These results paved way for a dynamical systems approach to turbulence. The interested reader is referred to [61] for a simple layman's discussion and [62] for a more technical treatment.

Since the seminal results of Ruelle and Takens, much work has been done in studying turbulence from the chaotic standpoint. More than a century after Reynolds discovered travelling wave structures in pipe flows prior to onset of turbulence [57], B. Eckhardt and co-workers explained the structures and subsequent transition to turbulence using a nonlinear model that was also validated experimentally [37] in 2004. In some instances the hydrodynamic and dynamical systems approaches have been applied synergistically to attack the structure of the energy cascade [3] using multifractal wavelet analysis and the intermittency problem as in case of the multifractal model [53].

In the past few years dynamical systems theory has become more generally applicable to a broader class of nonlinear and nonequlibrium systems leading to important results such as the Fluctuation Theorem of Cohen and Gallavotti [32] which leads to an extension of the equilibrium fluctuation-dissipation theorem [7, 39] to the nonequilibrium steady state condition. Some of the work discussed here bears heavily upon these recent ideas and tests them in compressible turbulence on a free surface. For an illuminating discussion of the present status of Nonequilibrium Physics and the underlying theory, the interested reader is referred to [19, 60].

1.2 STRUCTURE.

This dissertation may be broadly bifurcated in two parts. Part I involves two experiments discussed in chapters 2 and 3 that take the more traditional hydrodynamic approach to turbulence where Kolmogorov's theory of 1941 (K41) forms the basis for all analysis (see Appendix C for a brief discussion of the main aspects of K41).

Chapter 2 discusses an experiment conducted in incompressible turbulence in a large tank of water maintained in a turbulent steady state. A time-local version of the four-fifth law is applied to extract the instantaneous downscale energy transfer rate within the inertial sub-range of turbulence. The intent of this study is two-fold. First, it studies the finite size dependence of the system on fluctuations in the turbulent energy flux, with particular focus towards frequency of backscatter events. Second, it tests the validity of the recent Smooth Particle Hydrodynamics (SPH) method, an approximation proposed by Pumir et. al [56, 55]. The experimental analysis as well as the supporting numerical simulations provide a study of the size dependence on flux fluctuations. In addition, the time-traces of energy flux as obtained experimentally from the four-fifth law and from SPH method applied on experimental data are cross-correlated to test the validity of the SPH method. The high degree of correlation provides experimental proof of the accuracy of the SPH approximation. The supporting numerical simulations by the SPH method were conducted by A. Pumir.

Chapter 3 discusses an experiment involving compressible turbulence on a free surface. Despite the inapplicability of K41 to turbulence on a free surface (surface flow being compressible, an essential requirement of K41 is violated), Cressman et. al. [18] discovered that the Eulerian structure functions of velocity differences at the surface exhibit scaling consistent with K41. However the third-order structure function was not measured in previous measurements. It is measured here and shown to agree very well with the four-fifth law, suggesting that the surface might participate in an energy cascade process despite violation of the incompressibility condition. Analysis is also conducted in the Lagrangian frame of reference (see section 2.2 for defintion). In the absence of suitable theoretical guidance, there are no *a priori* expectations from this experimental analysis. Given the agreement of Eulerian statistics with K41, the second-order lagrangian structure function is measured to

see if it scales linearly in time in accord with K41. This function is instead found to scale as a power-law in time with exponent 1/2. It is not clear if this exponent is indeed 1/2, or comes about from compounded intermittency effects due to surface as well as lagrangian measurements. No reliable scaling is observed for higher-order structure functions due to limited statistics.

In Part II which consists of two experiments, the emphasis is upon the chaotic character of turbulence. Here turbulence is applied as a chaos-generating mechanism to study the nonequilibrium dynamical aspects such as measurement of the steady state entropy production rate and testing its fluctuations against the steady state fluctuation theorem of Gallavotti and Cohen.

Chapter 4 is an experiment designed to test the recent theory of Falkovich and Fouxon to measure the steady state entropy production rate in compressible turbulence at a free surface. The measured entropy rate is predicted to equal the time integral of the lagrangian velocity divergence correlation function with a negative prefactor. This function is measured for the first time, but the results are found not to be in accord with theory. The theory also predicts the entropy rate should equal the sum of the system's Lyapunov exponents which are obtained from numerical simulations by Boffetta et. al. under driving conditions very similar to that of the experiment. The measured entropy rate from the experiment agrees very well with the sum of Lyapunov exponents from simulations.

The Steady State Fluctuation Theorem is an important theoretical result to emerge in recent years for systems in the nonequilibrium steady state. In Chapter 5, the lagrangian velocity divergence of individual particle trajectories from the dataset in Chapter 4 is interpreted as the local entropy rate. Its fluctuations are put to test against the Fluctuation Theorem of Gallavotti and Cohen. The results are found to overshoot the theoretical prediction at early averaging times, and undershoot the prediction at late averaging times. In an intermediate window of averaging times the measurements fit extremely well with the Fluctuation Theorem over an extended range before abruptly deviating from the theoretical prediction. There are quite a few novel aspects in this study. This is the first experiment to test the Fluctuation Theorem in lagrangian frame. Second, the test is conducted for a quantity that is not the thermodynamic entropy rate, but pertains to the dimensionless en-

tropy studied in the context of chaotic dynamical systems. Third, when in agreement with the Fluctuation Theorem, the results extend over a range not spanned by prior experiments and simulations, and fourth, the experiment clearly demarcates averaging time-scales where the Fluctuation Theorem works and where it fails.

Finally, the results are summarized in Chapter 6, followed by a discussion of future possibilities amenable to experimental analysis with some initial thoughts on how to conduct such experiments.

2.0 ENERGY FLUX FLUCTUATIONS IN INCOMPRESSIBLE TURBULENCE.

2.1 INTRODUCTION.

Incompressible turbulence in three-dimensions (3D) is characterized by a cascade of energy from large to small spatial scales. The energy cascade originates at the largest scales of turbulence close to the energy injection scale. More specifically, it originates at the largest scale where velocity fluctuations in the fluid are spatially correlated. This spatial scale is referred to as the integral or outer scale (l_0) of turbulence. The energy entering at the integral scale undergoes successive transfer to smaller scales until it reaches the smallest scales of turbulence, where it undergoes viscous dissipation into heat. This smallest scale of turbulence is commonly referred to as the inner, dissipative, or the Kolmogorov scale (η). The range of spatial scales between the outer and inner scales ($l_0 \gg r \gg \eta$) that participate in the energy cascade are collectively referred to as the inertial sub-range, owing to the fact that the inertial terms of the Navier-Stokes equation dominate the dissipative terms in this region. No dissipation is expected to take place in the inertial sub-range.

The cascade interpretation of turbulent energy transfer finds its first references as early as 1922 in the works of L. F. Richardson [58]. However, present understanding of the turbulent energy cascade derives its basis from the Kolmogorov four-fifth law [38, 29].

$$\langle [\Delta u_L(r)]^3 \rangle = -\frac{4}{5}\overline{\varepsilon} r \tag{2.1}$$

Here $\langle ... \rangle$ represents an ensemble average and $\Delta u_L(r) = (\mathbf{u}(\mathbf{x}+\mathbf{r}) - \mathbf{u}(\mathbf{x})) \cdot \mathbf{r}/r$ is the longitudinal velocity difference between two points in the fluid separated by a distance r. $\overline{\varepsilon}$

represents the average energy transfer rate at the given scale r. The negative sign in the four-fifth law implies a transfer of energy downscale from large to small r. Eq. (2.1) holds only for the inertial range of spatial scales ($l_0 \gg r \gg \eta$) . For $r \simeq \eta$ an additional term, also derived by Kolmogorov, makes its appearance felt [29]. The four-fifth law is derivable under conditions of isotropy, homogeneity and incompressibility of the turbulent fluid in question. It is one of the most important results in fully developed turbulence because it is both exact and non-trivial. For a brief discussion of the four-fifth law in the context of K41, please see Appendix C.

The spatially averaged value of the energy flux ε over a subvolume of the fluid B of typical size R is simply given by the rate of dissipated kinetic energy if the system is in a steady state. In that case the flux is necessarily positive and is directed from large to small scales. However, temporal fluctuations in this flux can be very substantial. In fact, it has been demonstrated several times that energy may backscatter from small to large scales, leading to a *negative* value of the energy flux [68, 43]. It is natural to expect that this effect should depend on the scale of the subsystem investigated. One of the aims of this study is to quantify the fluctuations of the energy flux measured over a subdomain of the flow, and in particular, its dependence on the subdomain's size. The experimental observations are corroborated by a numerical simulation based on the motion of many particles and on an explicit form of eddy damping.

2.2 THEORY.

Under conditions of local isotropy, the ensemble-averaged energy dissipation rate, $\overline{\varepsilon}$, is related to the third moment of longitudinal velocity differences at a given scale, r (LHS of Eq. (2.1), henceforth called $S_3(r)$). The recent theoretical [51, 20, 23] and supporting numerical work [71] leads to a generalization of Eq. (2.1), which is local in space and time. More precisely, if one considers any finite subdomain, B, the average of $[\Delta u_L(r,t)]^3$ over all directions of the vector $\mathbf{r}$, and over all points in B, is equal to $(-4/5)\varepsilon_B(t)r$, where ε_B is the energy flux

towards small scales in the subdomain B,

$$\varepsilon_B(r,t) = \frac{1}{2}\frac{d\langle v^2(r)\rangle}{dt} = \frac{\langle[\Delta u_L(r,t)]^3\rangle_{B,\Omega}}{-\frac{4}{5}r} \tag{2.2}$$

Here $\langle ...\rangle_{B,\Omega}$ denotes the average over the subvolume B, and over all possible directions (Ω), and $\langle ...\rangle$ around v^2 denotes an average over all velocity vectors in an instantaneous snapshot. This subvolume is a finite box of side length R. The derivation of Eq. (2.2) is based on a rigorous energy balance for weak solutions of the Navier-Stokes equation, in the $\mathrm{Re} \to \infty$ limit [20]. In this sense the quantity $\varepsilon_B(t)$ is really the instantaneous, inertial range dissipation rate, interpreted here as an energy flux (defined as positive towards small scales). Equation. (2.2) justifies the intuitive estimates of the rate of change of energy in a volume, by a straightforward averaging with the help of Eq. (2.1), even when the key assumption of local isotropy is not satisfied. The spherical average in Eq. (2.2) permits the recovery of the isotropic sector from an arbitrary (anisotropic) flow [71] via preferential weighting along specific directions which are deduced from the directionality of the flow. The non-requirement of flow isotropy, and the fact that Eq. (2.2) is rigorously derived to hold locally in time, makes it a more general derivation of Eq. (2.1), and constitutes a stronger statement concerning the rate of energy transfer within the inertial sub-range.

As will be discussed in section (2.4.1), in practise the average over all directions is replaced in the experiment by a weighted average over particle pairs along all azimuthal directions in an instantaneous snapshot within a subdomain B of interest. The magnitude and sign of the numerator on the right-hand side (RHS) of Eq. (2.2) fluctuates in time, though it must be negative on the average if the system is in the steady state. This assures that the time average of the flux $\varepsilon_B(t)$ is positive.

Averaging over all pairs of particles in a subdomain of the fluid, as done in the experiment, has also been proposed as a way of estimating the energy dissipation in a numerical scheme, based on the "Smooth Particle Hydrodynamics" (SPH) method [46]. In such an approach the values of various hydrodynamic fields at a point x are obtained by interpolating, with the help of all the neighboring particles, within a smoothing distance h from the point x. An expression for the eddy damping, very similar to Eq. (2.2) has been postulated in [55]. Implementing this eddy damping numerically in an SPH code, as done in [55] leads to a large

eddy simulation scheme, based on particles moving with the flow (Lagrangian particles), where the smoothing length h is the smallest scale resolved numerically. The experimental setup to be discussed in section (2.3) allows an explicit measurement of the energy flux from Eq. (2.2) and a comparison with the postulated form of the eddy damping [55]. As will be shown in section (2.5), the experimental results demonstrate that the postulated form of the energy-dissipation term is very strongly correlated with the energy flux obtained from Eq. (2.2). Furthermore, the numerical scheme based on SPH allows one to study the energy flux in a subdomain of the system as a function of size.

2.3 EXPERIMENT.

The experimental setup is shown in Fig. 2.1. Measurements are made 4 cm below the surface in a square tank of side length 1 m, filled with water to a height of 30 cm. The fluid is seeded with neutrally buoyant glass beads of 10 μm diameter. The local velocity of the fluid is captured by a high speed camera (Phantom v5.0) that records the movement of particles over a square area of side length $L = 7.7$ cm. A beam of laser (5.5 Watt Verdi solid state laser) is passed through a cylindrical lens to generate a sheet that cuts through a plane in the bulk fluid 4 cm below the surface. The laser sheet is roughly 1 mm thick, but the camera's depth of field is a tenth of this. Thus only horizontal components of velocity are captured. The buffer size of the camera limits the duration of data collection to 5 s at a frame rate of 400 frames per second. The velocity field is constructed by correlating pairs of images with a particle tracking program [59]. The spatial resolution of the measurements is dependent upon the length of a pixel in the camera's charge-coupled device (CCD) sensor. Hence the spatial resolution in this experiment is 7.7 cm/1024 pixels = 75 μm. The temporal resolution is the sampling rate which is 7.5 ms for this experiment. Hence the velocity resolution obtained in this experiment is 1 cm/s. To ensure reliability of the measured velocities, every n^{th} and $(n+3)^{rd}$ image is employed in velocity field construction. The weak nonzero mean velocity observed in the flow is systematically subtracted out. Physical parameters that characterize turbulence in this experiment are given in table 2.1.

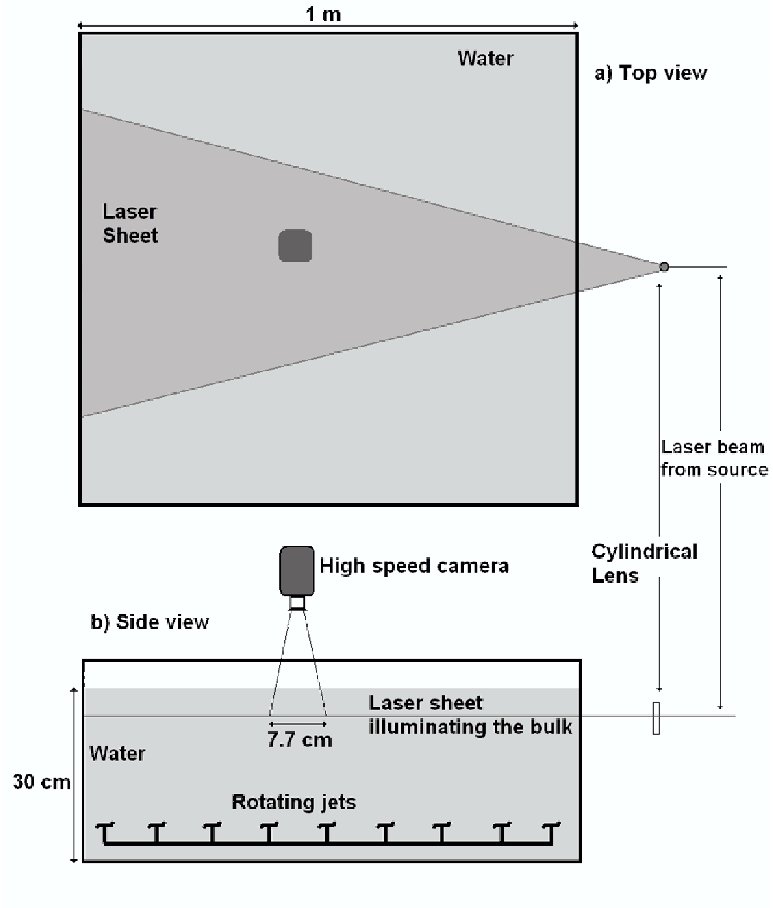

Figure 2.1: a) Top view and b) Side view of the experimental setup. A tank of lateral dimensions 1 m x 1 m is filled with water to a depth of 30 cm. A laser beam passing through a cylindrical lens generates a sheet of laser that illuminates a horizontal plane of the turbulent fluid 4 cm below the surface. Turbulence is generated by a system of 36 capped rotating jets situated at the tank floor. Neutrally buoyant tracer particles are suspended in the turbulent fluid. A high speed camera suspended above the tank records the motion of tracers as they scatter light upon entering the sheet of illumination.

Table 2.1: Turbulent quantities of interest measured in the experiment.

Parameter	Expression	Measured Value
Taylor Microscale λ (cm)	$\sqrt{\frac{u_{rms}^2}{\langle(\partial u_x/\partial x)^2\rangle_x}}$	0.32
Taylor Microscale Reynolds Number Re_λ	$\frac{u_{rms}\lambda}{\nu}$	79
Integral Scale l_0 (cm)	$\int dr(\frac{\langle(u_L(x+r)u_L(x))\rangle_x}{\langle u_L(x)^2\rangle_x})$	3.5
Large Eddy Turnover Time τ_0 (s)	$\frac{l_0}{u_{rms}}$	1.4
Dissipation Rate ε_{diss} (cm^2/s^3)	$15\nu\langle(\frac{\partial u_x}{\partial x})^2\rangle_x$	8.3
Kolmogorov Scale η (cm)	$(\frac{\nu^3}{\varepsilon_{diss}})^{1/4}$	0.02
RMS Velocity u_{rms} (cm/s)	$\sqrt{\langle u(x)^2\rangle_x - \langle u(x)\rangle_x^2}$	2.4

2.3.1 ADVANTAGES AND DISADVANTAGES OF THE EXPERIMENTAL SCHEME.

The experimental setup was originally designed to study compressible turbulence on a free surface, and not incompressible bulk turbulence. However, the scheme presents some relative advantages with respect to other popular schemes (eg. pipe flows and wind tunnels, counter-rotating flows or the french-washing machine etc.) in use elsewhere.

1) The capped jets on the tank floor form the energy injection source to the turbulent body of water within the tank. The 2D plane of observation (4 cm below the surface) is roughly 26 cm above the injection source. This allows sufficient mixing of water thereby making the turbulent intensity quite homogeneous at the observational plane. This scheme also generates a fairly isotropic flow, although this is no longer a requirement under the derivation of Eq. (2.2). This is not so in case of other popular turbulence generating schemes. For instance, pipe flows and wind tunnel [50] experiments are not isotropic, and the french-washing machine scheme [67, 78] neither produces homogeneous turbulence nor is the flow isotropic.

2) A serious advantage enjoyed by the setup discussed in present experiments is the ability to reliably track a large number of tracer particles over an extended area. For the

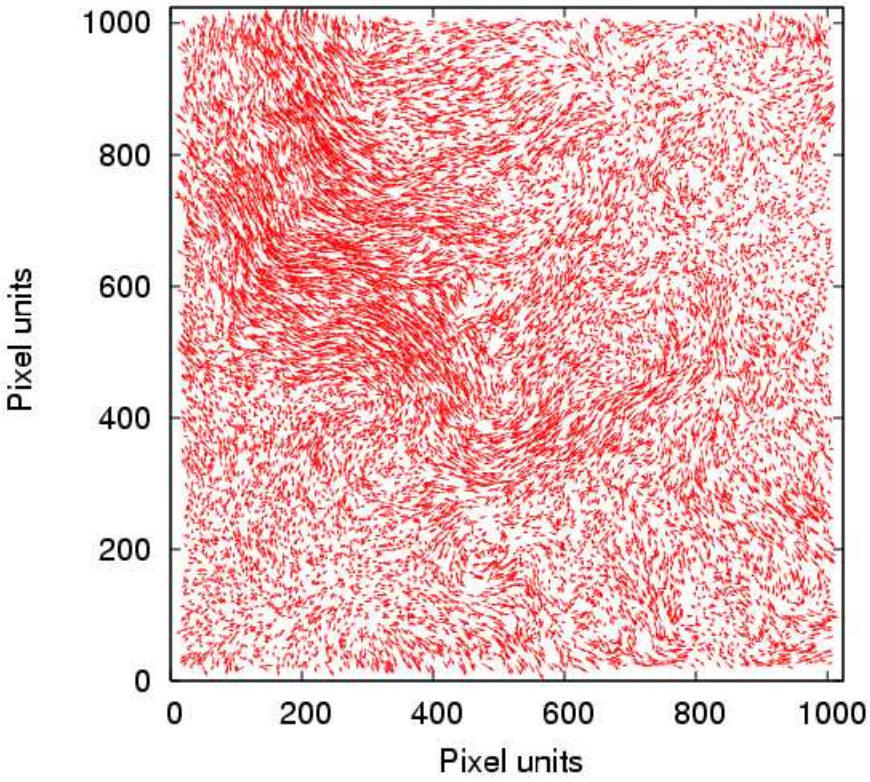

Figure 2.2: A snapshot of the instantaneous velocity field as constructed by the particle tracking program from raw data obtained in this experiment. The field is plotted in pixel units.

data applied in the analysis to follow, 14000 particle velocity vectors were reliably measured at each instant over an area 7.7 cm $\times$ 7.7 cm, providing $\frac{1}{2}14000 \times 13999 \simeq 10^8$ instantaneous particle pairs for the calculation of $S_3(r,t)$. Hence the scheme presents a distinct statistical reliability for measurements. Other schemes are only now beginning to realize such experimental capability. In the past, experimentalists have employed hot-wire probes for indirect measurement of velocity fluctuations through fluctuations in heat dissipated by a thin filament probe inserted in the turbulent flow. The probes provided time-traces of velocity fluctuations at a single point in space of the turbulent flow. The time traces were then converted into spatial units by applying the Taylor's hypothesis or the frozen turbulence assumption [29]. For applicability of the Taylor's hypothesis to the turbulent flow in question, it becomes necessary that the RMS (Root-Mean-Square) velocity fluctuations be far smaller than the mean velocity of turbulent flow [29, 78]. This is however not a concern in the present experiments, since the absence of mean flow invalidates application of the frozen turbulence assumption. Moreover, the present study requires simultaneous spatial and temporal measurements. This is made possible only by obtaining spatial velocity fields at each instant. This would not be possible with hot wire anemometry. Hence the particle tracking scheme employed here plays a crucial role in being able to simultaneously measure $S_3(r,t)$ in space and time.

There is however a serious disadvantage with the present scheme. Whereas wind tunnels, pipe flows and counter-rotating flows are capable of achieving Taylor Microscale Reynolds numbers upto 1200, and sometimes even 5000 (liquid helium in counter-rotating geometry [67, 78]), the scheme employed here only manages modest Microscale Reynolds numbers (Re_λ) of 79 (for a defintion of the Taylor Microscale please refer to [29] and Table 2.1). Convergence of $S_3(r)$ with the 4/5 coefficient in either Eq. (2.1) or Eq. (2.2), requires very high Reynolds numbers. The basis for this argument lies in the fact that at low Reynolds numbers, the inertial sub-range is not very well developed and becomes contaminated by injection scale effects. The inertial sub-range becomes more well defined with increasing turbulent intensity, or increasing Reynolds number. Owing to the modest Reynolds number at which the experiment was conducted, this point should be borne in mind while conducting all analysis, the implications of which will be discussed in the next section.

2.4 ANALYSIS.

2.4.1 CALCULATION OF MOMENTS.

The moments are calculated directly from the experimental velocity fields. $S_3(r)$ in Eq. (2.1) being an odd moment of velocity differences can take both positive and negative values. A large number of measurements are required in order to achieve reasonable statistical significance. As mentioned in section (2.2.1), such statistical significance was achieved in past experiments by collecting data for very long time intervals and subsequently applying Taylor's hypothesis [29] to convert the data into spatial units for calculation of moments. Since present experiments concentrate on temporal fluctuations of $S_3(r,t)$ in Eq. (2.2), long time averages are not allowed. Instead one is required to achieve good statistical significance in each snapshot of the experimental velocity fields. Fortunately, this is not a problem as the particle tracking method provides on the average 14000 velocity vectors per snapshot, thereby providing 10^5 particle pairs for each r-value of $S_3(r,t)$.

The velocity differences are calculated in the following manner. Taking each particle as the origin in the instantaneous snapshot of velocity field, two concentric circles of radii r and $(r+\Delta r)$ are considered such that the fractional area $(r/\Delta r)$ remains a constant. By trial and error, the smallest fractional area that could provide statistical signficance is found to be 0.05. All particles within the concentric area are then considered for calculation of velocity differences with the particle at the origin. This process is repeated for every particle in the instantaneous velocity field, adequate care being taken not to double count particle pairs. Repeating this procedure over all velocity field snapshots, one obtains a fluctuating time-trace of $S_3(r,t)$. That the third-moment can be reliably constructed at each instant for all r-values is understood from the fact that the integrand of the third-moment for an instantaneous snapshot is very well resolved as shown in fig. 2.5. The method described is equivalent to averaging along all azimuthal directions in the two-dimensional plane of observation, and is analogous to the spherical averaging scheme. A small amount of flow anisotropy observed in the experiment was systematically eliminated by subtracting out the mean velocity at each spatial scale by defining the third-moment of velocity differences as

$S_3(r,t) = \langle[\Delta u_L(r,t) - \langle\Delta u_L(r,t)\rangle]^3\rangle$.

2.4.2 TEMPORAL FLUCTUATIONS IN THE ENERGY FLUX.

Though the Reynolds number in this experiment is low (see Table 2.1), the flow exhibits a well-defined inertial range. Figure 2.3 shows the space and time-averaged $S_3(r)$ *vs.* r in the range 0.07 cm $\leq r \leq$ 3.5 cm. Each instantaneous third-moment is constructed from an average over all particle pairs in the field of view. Twelve time-uncorrelated measurements of the third-moment are averaged to obtain the plot in Fig. 2.3. The interval between these measurements is 1.4 s, which is the lifetime of the largest eddies, as determined from the velocity autocorrelation function. Therefore each data-set provides 4 measurements uncorrelated in time. Three such data-sets are taken in quick succession to obtain the average. In forming this spatial average of $S_3(r)$, data for $r <$ 0.07 cm are excluded, since velocity differences cannot be reliably measured below this value. The statistical error in the time averaged $S_3(r)$ is less than 5% as observed from the error bars in fig. 2.3.

Since the experiments are conducted in steady state turbulence, it is natural to expect that the space and time-averaged $S_3(r)$ should be proportional to the time-averaged energy dissipation rate calculated from velocity gradients. More specifically the ratio $S_3(r)/(-4/5\varepsilon_{diss}r)$ (ε_{diss} is the rate of energy dissipation as calculated from velocity gradients, see Table 2.1) should be a horizontal line with no slope within the inertial range of spatial scales. This statement merely translates to the expectation that in the steady state the average energy flux $\overline{\varepsilon}$ through the inertial range equals the average rate of dissipation at the Kolmogorov scale (η). The Kolmogorov scale η in the experiment is estimated (refer table 2.1) to be 0.02 cm. Whereas this scale can be reached in the present experiments, measurements out to $r =$ 0.07 cm fall within the range of experimental error, and hence are not reliable. It is therefore not possible to obtain an accurate estimate of velocity gradients at the Kolmogorov scale. Since velocity gradients represent spatial derivatives, the experimental velocity fields are binned into a 2D grid for calculation of spatial derivatives. The bin size is estimated by the smallest length scale which can accomodate at least one velocity vector per bin. The square root of the total area in pixels (1024^2) divided by the average number of velocity

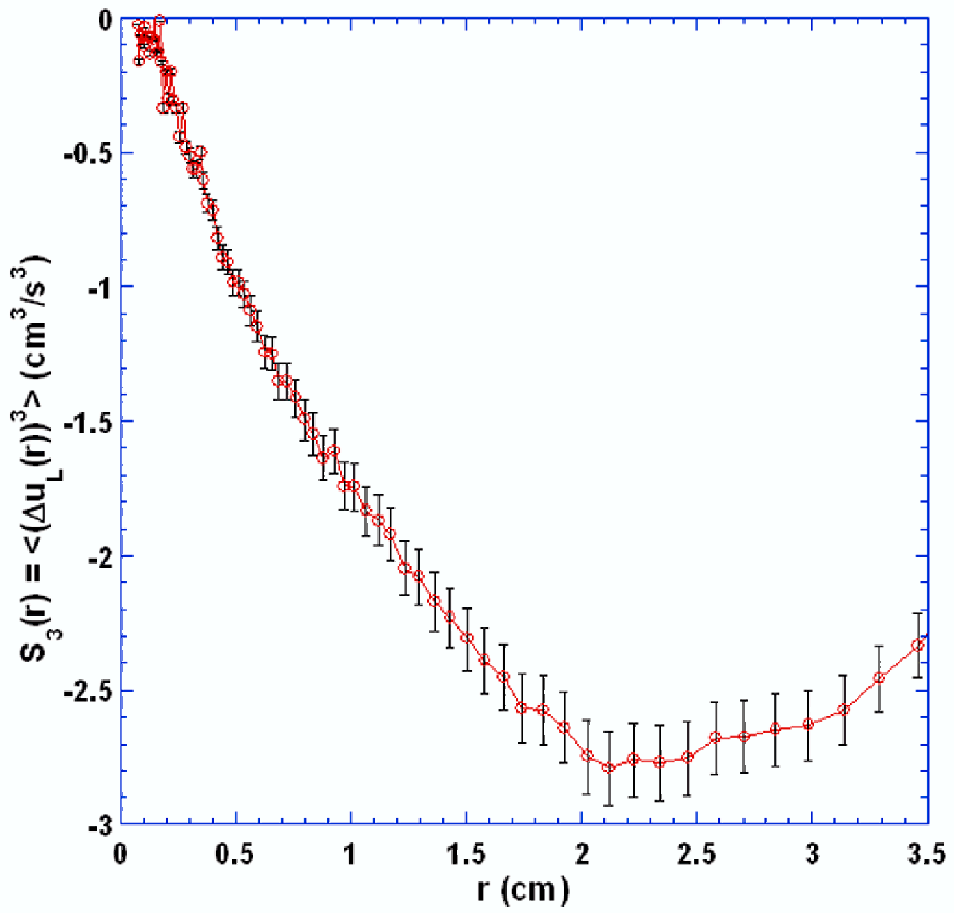

Figure 2.3: The time averaged third-moment of longitudinal velocity differences ($S_3(r)$) as a function of particle separation r (cm). The plot is constructed by averaging over twelve time-uncorrelated velocity snapshots.

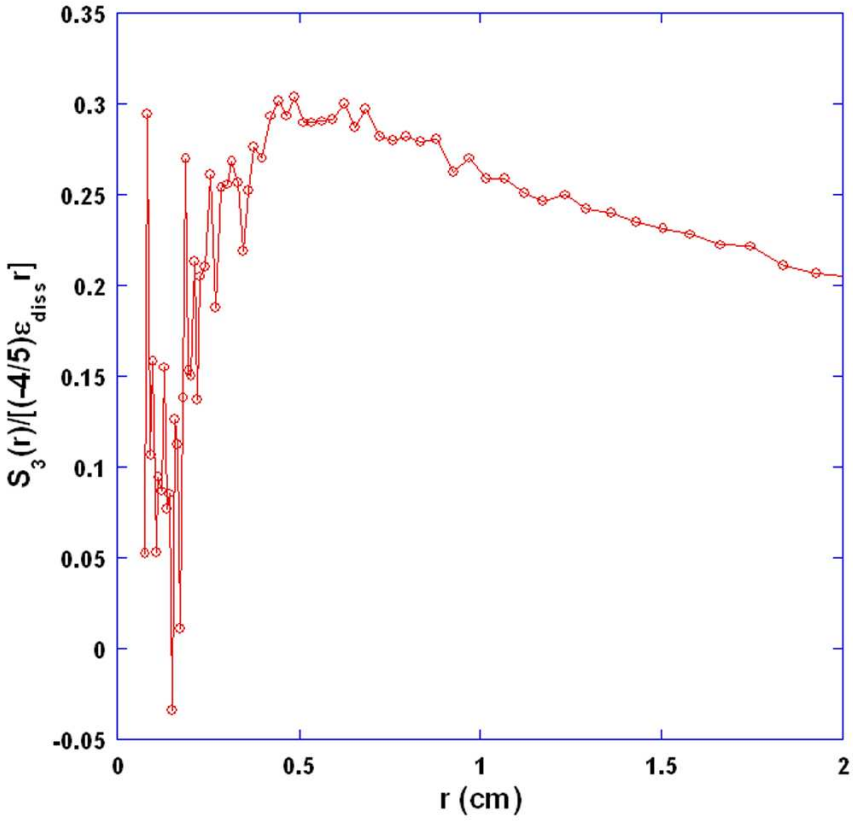

Figure 2.4: The ratio $S_3(r)/(-4/5)\varepsilon_{diss}r$ vs. r shows a limited range of spatial scales between r = 0.3 cm and 0.8 cm with zero slope. However, the ratio within this region is 0.3 and not 1 as one would expect.

vectors per velocity field (14000) provides an estimate for the side-length of the 2D bin to be $\sqrt{(1024)^2/14000} \simeq 8$ pixels. However, as a safe measure each bin is taken with a side-length of 10 pixels corresponding to $\frac{7.7\ cm}{1024\ pixels} \times 10\ pixels = 0.075\ cm$. This in turn ensures that the spatial derivatives are free of experimental error. Taking spatial derivatives of the binned velocity fields, the average dissipation rate may be estimated by applying the formula in table 2.1. Figure 2.4 plots the ratio $S_3(r)/((-4/5)\varepsilon_{diss}r)$ *vs.* r. As expected the plot shows a limited range of spatial scales between $r = 0.3$ cm and $r = 0.8$ cm within the inertial sub-range with zero slope. However, the ratio within this spatial region is not 1 as would be expected in the ideal case, but instead is about 0.3. This discrepancy in the expected ratio is attributed to two reasons. First, the experiment is conducted at a modest Reynolds number of 79, hence statistical convergence with the $4/5^{th}$ coefficient in Eq. (2.1) is not achievable. Indeed, even at very high Reynolds numbers, the convergence is found only within a limited region of the inertial sub-range [67, 66, 50]. Second, the average rate of dissipation is not an accurate measurement in this experiment since the velocity gradients could not be estimated at the Kolmogorov scale $\eta = 0.02$ cm, but were instead estimated at 0.07 cm, which (strictly speaking) lies in the inertial sub-range. Hence the average dissipation rate only serves as an order of magnitude estimate and not as an accurate quantifier.

Shown in Fig. 2.5 is $x^3P(x)$ where $x = \Delta u_L(r,t)$ at the three indicated r-values 0.3 cm, 0.5 cm, and 0.7 cm. The measurements were made at one instant of time. The integral of this function over x is the the instantaneous third moment of interest. Each $P(\Delta u_L(r,t))$ is constructed from 10^5 particle pairs. The error in each of the curves is adequately small to yield a statistically significant value of the (fluctuating) third moment and hence the pdf of this moment $P(S_3(r))$, at least for the values of r listed above. According to Eq. 2.2, the pdf of the energy flux is then given by $P(\varepsilon) = P(S_3(r))/(-\frac{4}{5}r)$.

The inset to Fig. 2.6 shows a 5-second time record of $\varepsilon(r,t)$ for $R = 1.925$ cm (R being the side length of the square box B defined in Section 2.2). One sees that the energy flux is positive most of the time, but does show intervals of reversed energy flow. The figure itself shows the pdf of energy flux at the same three inertial range r-values of Fig. 2.5. One expects that in the inertial range all three curves should coincide, and they approximately do so. This r-independence in the inertial range is expected for the third-moment. The energy flux

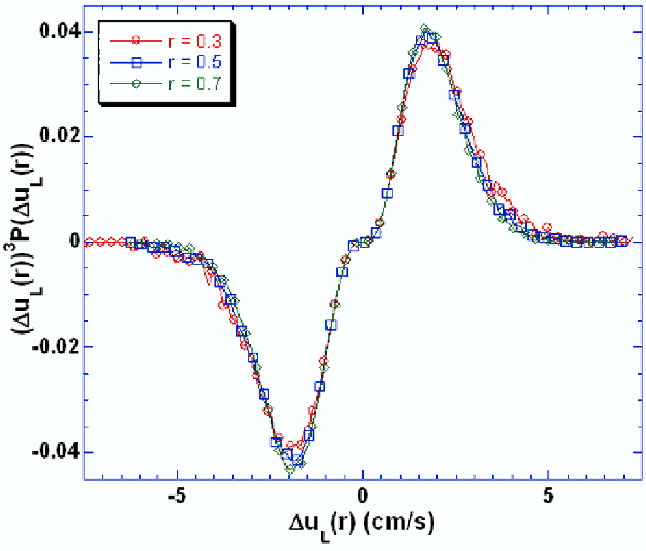

Figure 2.5: The integrand of the third-moment of longitudinal velocity differences can be constructed reliably for an instantaneous snapshot for different spatial separations r (here taken for r= 0.3, 0.5 and 0.7 cm).

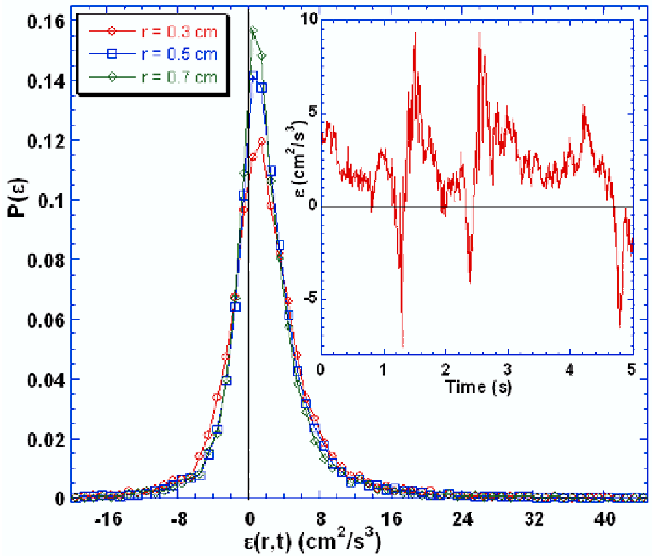

Figure 2.6: The inset shows the time trace of energy flux obtained from Eq. 2.2. The main figure shows the pdf of energy flux obtained for three different spatial separations r = 0.3, 0.5 and 0.7 cm within the field of view of side length R = 1.925 cm.

here is experimentally obtained from Eq. 2.2 for a sub-domain B of size $R = 1.925$ cm. As required by Eq. 2.2 the pdfs are positively skewed. This positive skewness is considered proof (private communication with C. Meneveau) of the preferred direction of energy transfer from large to small spatial scales in 3D incompressible turbulence.

The energy flux is also experimentally obtained for sub-domains B of size R ($R = 7.7$ cm, 3.85 cm and 1.925 cm) keeping the particle separation $r = 0.7$ cm constant. The "width" of their pdfs decreases with increasing R, as one would expect and is shown in fig. 2.7. In general agreement with previous observations, it is found that the probability of backscattering is significant, but it is measured to be a monotonically decreasing function of R when R increases beyond l_0.

2.5 SIMULATION.

The simulations were not conducted by the author. They were conducted by A. Pumir (Institut Non Lineaire de Nice and Universite de Nice). The author acknowledges the kind permission of A. Pumir to include details of the simulation in this work as they complement the experimental results using the SPH algorithm to simulate flows with particles [46]. In this approach, the fluid is represented by particles, whose positions, $\mathbf{r}_i$ and velocities, $\mathbf{v}_i$ evolve according to the equation of motion :

$$\frac{d\mathbf{r}_i}{dt} = \mathbf{v}_i \quad ; \frac{d\mathbf{v}_i}{dt} = -\nabla p_i + \mathbf{f}_i + \mathbf{D}_i \tag{2.3}$$

where ∇p_i is the pressure gradient, $\mathbf{f}_i$ the forcing term, and $\mathbf{D}_i = \overline{\varepsilon}_h$, the inertial range dissipation term to be discussed below in Eq. 2.4. The pressure is obtained from the local density ρ_i from the equation of state $p = \rho^\gamma$ ($\gamma = 9$), which corresponds to a very weakly compressible gas provided $|v_i|$ is small compared to the velocity of sound. The density ρ as well as the gradients are computed at a point $\mathbf{x}$ by interpolating the properties of the particles with a kernel function characterized by a size h. In this approach, scales smaller than h are unresolved. The SPH method allows one to simulate flows with a resolution no better than h.

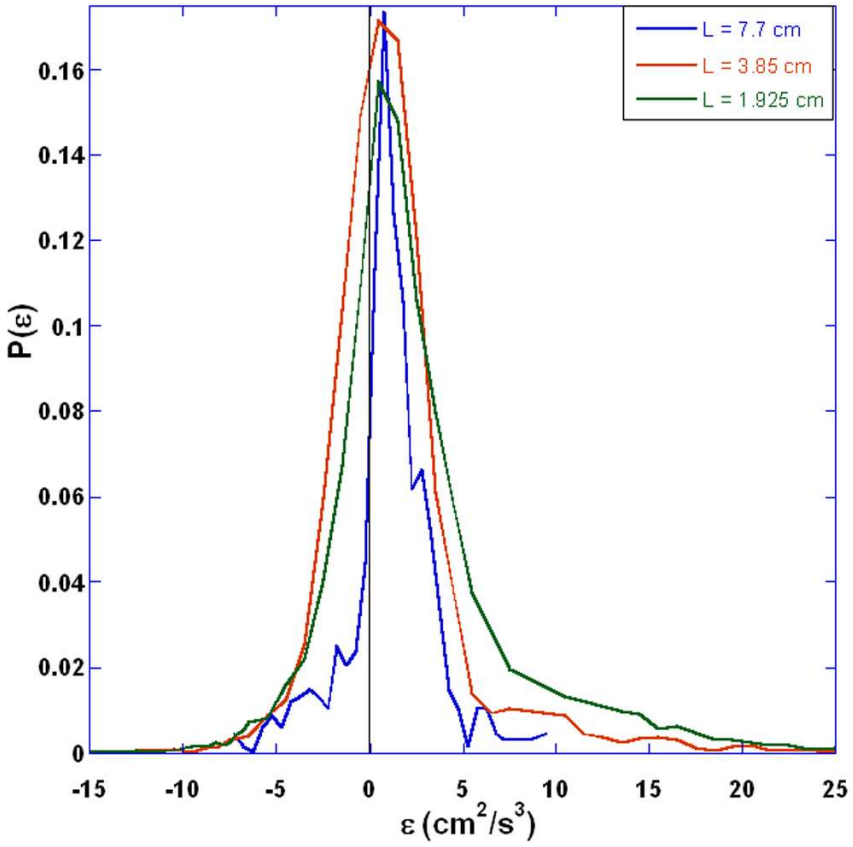

Figure 2.7: PDF of the energy flux ε as obtained for different sub-domains R = 7.7 cm, 3.85 cm and 1.925 cm and r = 0.7 cm. As seen the probability of backscatter decreasing with increasing sub-domain size. The backscatter probability was calculated to be 13% for sub-domain size of R = 7.7 cm, 17% for R = 3.85 cm and 25% for R = 1.925 cm, providing an approximate estimate of the decrease in frequency of backscatter events with increasing sub-domain size.

The issue is thus to adequately parametrize the sub-grid energy dissipation $\overline{\varepsilon}_h$ occuring below the scale h. The precise form for $\overline{\varepsilon}_h$ is inspired by the Kolmogorov equation [56, 55]; it corresponds to an energy dissipation of :

$$\overline{\varepsilon}_h = -\frac{\nu_t}{h^2}\langle(\mathbf{v}_{ij}.\mathbf{r}_{ij})\mathbf{v}_{ij}^2\rangle. \tag{2.4}$$

Here the angular brackets denote an average over all particles and this term is negative on the average, and $\mathbf{v}_{ij} \equiv (\mathbf{v}_i - \mathbf{v}_j)$ is the velocity difference between the particles i and j separated by the distance r_{ij}. The parameter ν_t is a dimensionless constant deduced to be of the order of unity [55], and should not be confused with kinematic viscosity. The experimental apparatus permits measurement of the postulated eddy damping term, and a comparison with the form of Eq. 2.2. Agreement between the flux in Eq. 2.2 and the dissipation in Eq. 2.4 is extremely good. With a properly adjusted value of ν_t, the correlation between $\varepsilon(t)$ and ε_h is $\sim$ 0.98 at the three values of R = 7.7, 3.85 and 1.925 cm. All the properties of the energy flux computed with Eq.(2.4) are essentially identical to the properties computed with Eq.(2.2), as shown in Fig. 2.9. The value of ν_t depends on the precise geometry of the subdomain B, and for the experimental geometry applied here, it was estimated to be 4.8. This experimental finding is a striking confirmation of the validity of the eddy-damping postulated in [55]. Figure. 2.8(b) shows the time-trace of energy flux $\varepsilon_{exp}(t)$ as obtained from the experimental data from application of Eq. 2.2. The same data was analyzed by the SPH approximation method of Eq. (2.4) and the time-trace $\varepsilon_{SPH}(t)$ is plotted in fig. 2.8(c). A mere visual inspection shows striking similarity between the two time-traces. In order to quantify the extent of this similarity, the two time-traces were temporally cross-correlated. This cross-correlation plot is shown in fig. 2.8(a). The normalized cross-correlation coefficient at $\tau = 0$ was calculated to be $\simeq 0.98$ thus proving that the eddy damping term postulated in [55] captures all essential features of the energy transfer in incompressible turbulence.

The implementation of SPH algorithm is described in [55]. In the calculation, the forcing term is chosen as a random superposition of three low-wavenumber fourier modes. The velocity of each particle was no larger than 1/10 the velocity of sound, so the flow is effectively incompressible. The energy flux over a sub-volume of the system is computed numerically,

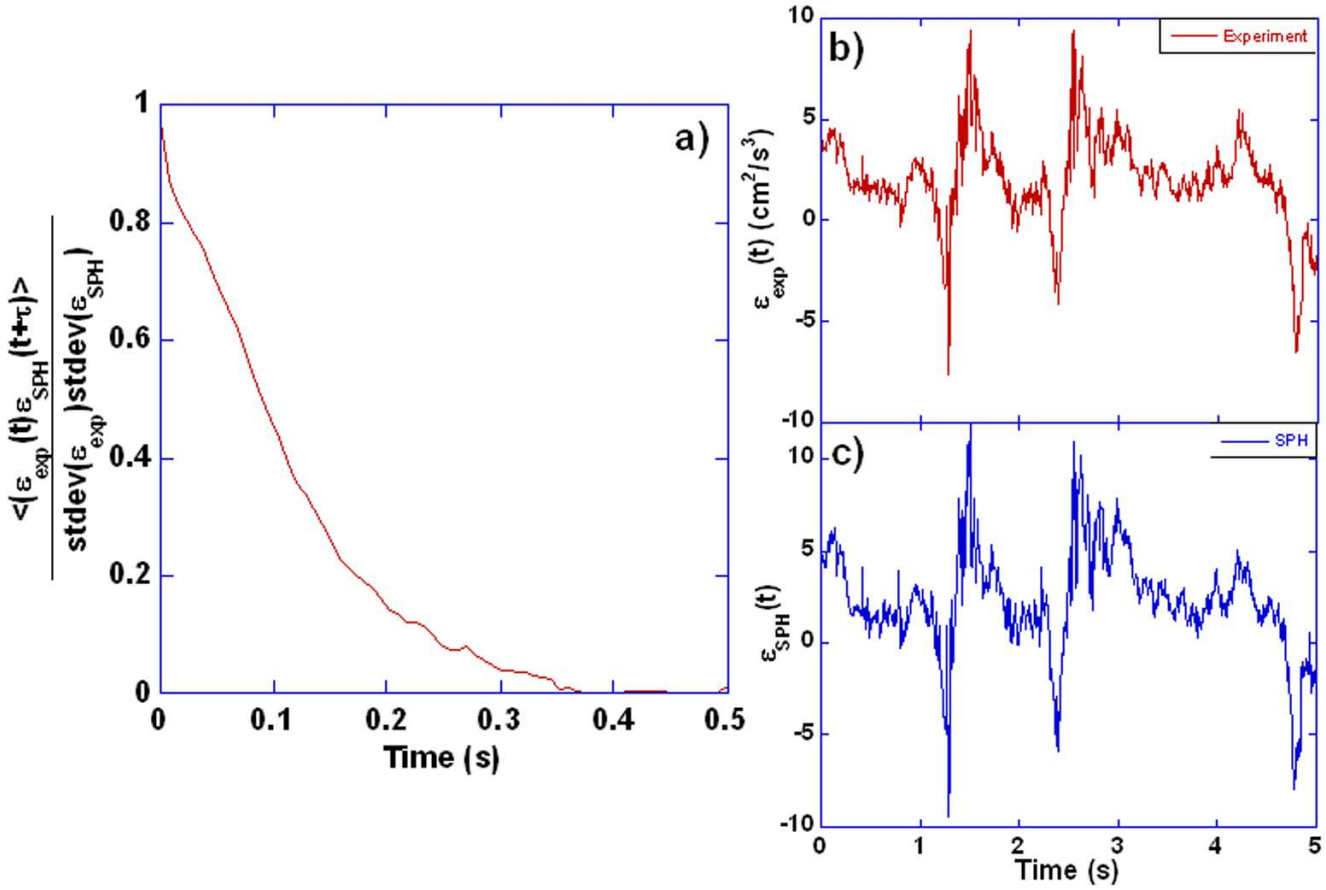

Figure 2.8: a) Temporal cross-correlation of the energy flux ε obtained from the experimental data from Eq. (2.2) and Eq. (2.4). The horizontal axis is the time τ in seconds. The two quantites exhibit a normalized correlation strength of 0.98 at $\tau = 0$ s. b) Time trace t, of energy flux obtained via Eq. (2.2) and c) as obtained by applying SPH approximation of Eq. (2.4). A mere visual inspection shows that the two time-traces are quite similar.

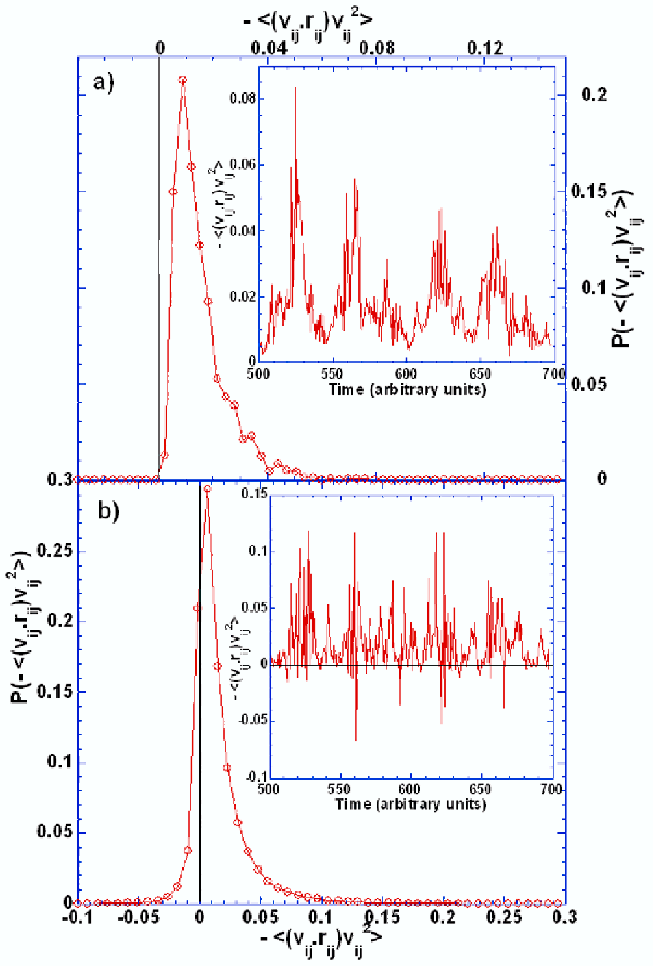

Figure 2.9: (a) Time-trace (inset) and the pdf of energy flux ($-\langle(\mathbf{v_{ij}}\cdot\mathbf{r_{ij}})v_{ij}^2\rangle$) for a simulation box of side length L/2. The fluctuations are always positive and never change sign. (b) Time-trace (inset) and the PDf of energy flux for a simulation box of side length L/8. The fluctuations switch sign frequently when the box size has diminished.

as effectively done in the experiment. The total energy flux averaged over a system volume of side-length L/2 (for a simulation box of side-length L) has large fluctuations. The inset to Fig. 2.9(a) shows that the fluctuations remain negative for as long as the simulations have been carried out. However, when averaged over a smaller fraction of the volume of side-length L/8, one finds that positive fluctuations of the averaged energy-flux become possible. This is evident from the inset to Fig. 2.9(b) and the corresponding pdf. The smaller the box size larger are the fluctuations. This finding is fully consistent with the experimental observations. As in the experiment, it was found that the probability of energy flux backscattering is a monotonically decreasing function of the scale R over which the flux is defined.

2.6 CONCLUSION.

Fluid turbulence research has focussed either on small scale properties, with the objective of understanding "intermittency", or on averages of global properties of interest for most applications. Only recently has a more systematic investigation of global fluctuations been undertaken [54, 12, 13]. The focus here is on the energy transfer to smaller scales, a hallmark of hydrodynamic turbulence. Whereas on average, the fluid transfers energy to smaller scales via the cascade process, the observed fluctuations are so large, as to actually reverse the energy flux from small to large scales [68]. This experimental study of the fluctuations of the energy flux is based on an experiment carried out at moderate Reynolds number. The results are based on Eq. 2.2. It has been shown that the probability of energy backscattering decreases when the size of the system increases. Also, the form of the eddy-damping term as proposed in [55] has been justified. The experimental results are corroborated by the results of the calculation based on the particle method.

3.0 SCALING ANOMALY BETWEEN EULERIAN AND LAGRANGIAN VELOCITY STATISTICS IN COMPRESSIBLE TURBULENCE ON A FREE SURFACE.

3.1 INTRODUCTION.

The clustering of foam or flotsam on a turbulent ocean's surface is a commonplace occurance. Such inhomogeneous distribution of matter due to turbulent advection is a generic consequence of compressible turbulence. However, the underlying turbulence in case of the ocean's surface is incompressible. The compressible effects at the surface of an incompressible turbulent fluid may be better appreciated from figure 3.1, where a homogeneous distribution of particles is introduced over the turbulent surface of water at $t = 0$. The density of the particles being less than water, they are trapped at the surface. As time progresses, the floaters quickly flee fluid up-wellings. They cannot follow the fluid into the bulk as water molecules do. As a result the floaters cluster into string-like structures around fluid down-wellings, thus leading to an inhomogeneous distribution. Of course, if neutrally buoyant particles were employed instead of floaters, no compressible effects would arise. The clusters evolve within a fraction of a second as seen in the figure, and the experiment itself is over within a second. The turbulence does generate ripples at the surface as one would expect, but their amplitude is small and can be neglected [33]. Additional effects arising from wave generated turbulence are not studied in this work.

The water on which the floaters move is incompressible at all values of z (vertical direction) including the surface ($z = 0$). The three-dimensional divergence of the velocity field is therefore identically zero everywhere (including the surface). However the two-dimensional velocity divergence at the surface is non-zero, since $\vec{\nabla}_2 \cdot \vec{v} = \partial_x v_x + \partial_y v_y = -\partial_z v_z \neq 0$. The

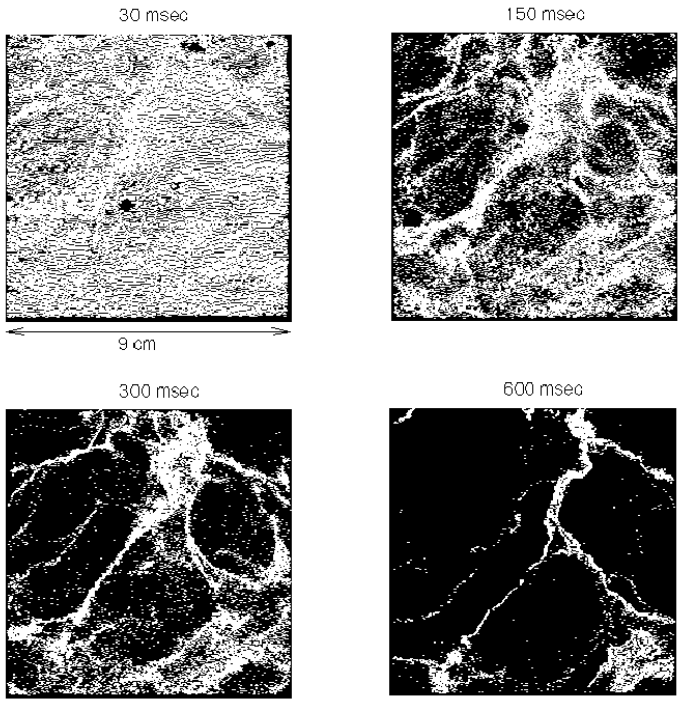

Figure 3.1: The evolution of particle clusters on a turbulent surface is shown for four snapshots in time as they evolve from a nearly homogeneous distribution at $t = 30$ ms towards an inhomogeneous distribution through $t = 150$ ms and 300 ms. The experiment is over by $t = 600$ ms, by which time particles have almost completely clustered into ribbon-like structures.

surface compressibility is quantified in a dimensionless measure expressed as $C = \frac{\langle(\vec{\nabla}\cdot\vec{v})^2\rangle}{\langle(\vec{\nabla}\vec{v})^2\rangle}$. If the turbulence is isotropic, the fluid is incompressible when $C = 0$, and completely compressible when $C = 1$. Previous experiments and numerical studies [18] have consistently measured $C = 0.5$ at the surface, thus ensuring the system is strongly compressible.

A short digression on frames of reference is necessary before explaining the problem to be studied in this analysis. In turbulence research one has the freedom to conduct studies in any one of two frames of reference, Eulerian and Lagrangian. When an experimental probe is kept fixed in space and measurements of turbulent quantities (say velocity or pressure) are made at that point in space, it constitutes an Eulerian measurement. In this reference frame temporally varying measurements are made at a single point in space as the fluid elements flow past the probe. In contrast, when an experimental probe moves with a fluid element (eg. tracer particle) that evolves under the action of turbulence and tracks its evolution, it constitutes a lagrangian measurement. A simple way of understanding the difference between the two frames is to realize that the Eulerian frame is equivalent to the lab frame of reference. The lagrangian frame is never fixed with respect to the lab frame but moves along with the evolving fluid element.

Structure functions that are measured in the Eulerian frame are referred to as Eulerian structure functions. These structure functions vary spatially from one Eulerian position to the other. Although all Eulerian measurements are temporally varying quantities at a single position, they can be converted into spatial quantities by applying the Taylor's hypothesis (see section 2.3.1). The primary predictions of K41 are made in the Eulerian frame ($S_3(r) = -4/5\bar{\varepsilon}r$ and $S_n(r) \sim (\bar{\varepsilon}r)^{n/3}$). In contrast Lagrangian structure functions are computed from an ensemble average over a large number of trajectories of tracer particles that evolve in time. These structure functions are temporal functions $D_n(\tau)$.

Unlike incompressible turbulence where Kolmogorov's theory [29] makes certain non-trivial predictions, there is currently no theoretical guidance to explain most phenomena observed at the surface. Kolmogorov's theory of 1941 is based on assumptions of isotropy, homogeneity and incompressibility of the turbulent flow in question. This theory is rendered inapplicable to turbulence at a free surface for various reasons that will be discussed in due course. Despite non-applicability of Kolmogorov theory for free-surface turbulence,

past measurements [18] have shown that the Eulerian structure functions of longitudinal velocity differences ($S_n(r) = \langle(\Delta u_L(r))^n\rangle$) exhibit scaling ($S_n(r) \sim r^{n/3}$) consistent with the Kolmogorov theory. Intermittency is admittedly higher at the surface [18] than within the incompressible bulk leading to anomalous exponents for higher order structure functions.

The extension of Kolmogorov's similarity hypothesis to the lagrangian frame in fully developed turbulence (see pages 358-361 of [47] for a simple discusssion, and section 4 of [77]) gives rise to two scaling predictions for the second-order Lagrangian structure function of velocity differences ($D_2(\tau) = \langle(\Delta u(\tau))^2\rangle$), depending upon the time scale τ at which measurements are made. For τ comparable to time-scales that correspond to the inertial sub-range ($\tau_\eta \ll \tau \ll \tau_0$, where τ_η is the dissipative time scale of the smallest eddies and τ_0 corresponds to the large eddy turnover time of turbulence)(see section 24.2, specifically pages 547-551 of [47] for derivation):

$$D_2(\tau) = \langle(\Delta u(\tau)^2)\rangle = C_0\bar{\varepsilon}\tau. \tag{3.1}$$

Here $\langle ...\rangle$ denote an ensemble average over many realizations of lagrangian trajectories. Eq. 3.1 is considered the Lagrangian counterpart for the four-fifth law as it scales linearly with time τ and the average rate of energy transfer $\bar{\varepsilon}$. However unlike the four-fifth law which is exact, Eq. (3.1) is only a scaling prediction arising from dimensional analysis. The primary assumption made in its derivation is the short-time correlation of lagrangian velocity acceleration in fully developed turbulence. At present no Lagrangian analog for the Monin-Kármán-Howarth relation (see section 6.2.1 of [29], a brief discussion is also given in Appendix C) exists, thus preventing one from deriving a relation similar to the four-fifth law in lagrangian frame. The failure of dimensional analysis in predicting the scaling forms for higher-order Eulerian structure functions is now well appreciated. The disagreement with predictions arising from Kolmogorov's self similarity hypothesis and experimental observations is attributed to intermittency effects at small scales of turbulence, and forms a subject of intense interest [2, 8, 45]. Since Eq. (3.1) comes about via dimensional arguments, its applicability even in incompressible turbulence demands a careful and cautious approach. When τ is shorter than the dissipative time scale τ_η the above relation does not hold. The correct relation for ($\tau \ll \tau_\eta$) is $D_2(\tau) = a_0\bar{\varepsilon}^{-3/2}\nu^{-1/2}\tau^2$ (see [47, 77]). The present experiment

concentrates on the inertial range time-scale where Eq. (3.1) holds provided the turbulence is incompressible.

There are no *a priori* expectations in this experimental analysis due to lack of a suitable theory to guide the experimentalist. All analysis therefore, proceeds through comparison with K41 which is strictly applicable for incompressible turbulence, but finds interesting agreements with the compressible flows studied here. In this experimental study velocity field data collected for compressible turbulent flow at the surface is analyzed in both Eulerian and Lagrangian frames of reference with specific focus towards the third-order Eulerian structure function and the second-order Lagrangian structure function. It is observed that the third-order Eulerian structure function $S_3(r)$ exhibits **very good** agreement with Kolmogorov's four-fifth law despite violation of the incompressibility requirement. This is in agreement with Kolmogorov scaling observed for Eulerian structure functions of order other than $n = 3$ measured previously [18]. This is the first time the third-order Eulerian structure function has been measured in surface turbulence. The linear scaling of $S_3(r)$ in space is suggestive of an energy cascade process at the surface. Assuming applicability of the four-fifth law at the surface, the analysis for energy flux fluctuations (Chapter 2) is repeated here for surface measurements. The PDF of energy flux fluctuations is qualitatively similar to the one observed for incompressible turbulence.

The strong agreement of $S_3(r)$ with four-fifth law forms the only basis that allows one to "hope" that the second-order Lagrangian structure function $D_2(\tau)$ might scale linearly in time τ from Eq. (3.1). The reasons for inapplicability of Eq. (3.1) are however more compelling. What is surprising though, is that the experimental results show a power-law scaling form ($D_2(\tau) \sim \tau^{1/2}$). The results present a serious scaling mismatch between the Eulerian and Lagrangian structure functions. Given the inapplicability of Kolmogorov theory and a suitable alternative theory being unavailable, interpretation of the results remains inconclusive. Some physical arguments are presented to explain this scaling anomaly. The arguments do however require either a sound theoretical framework, or definitive experiments to prove their validity.

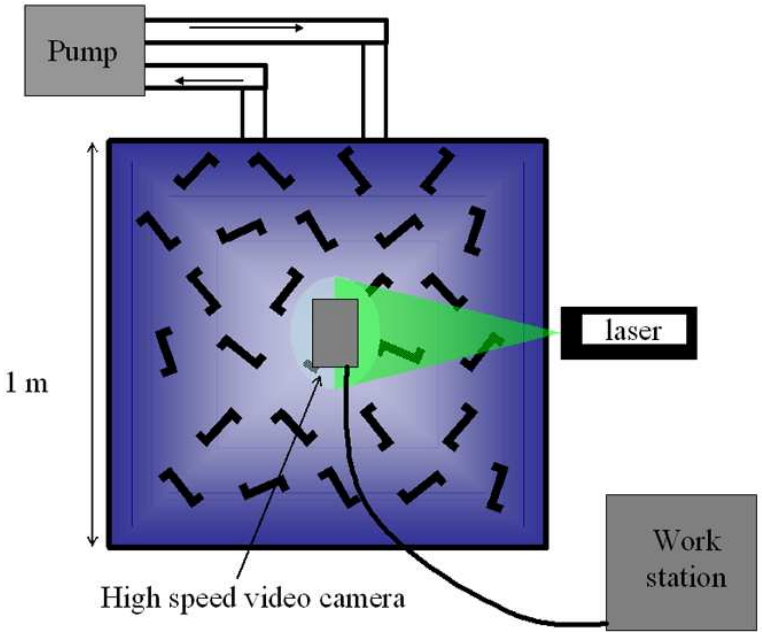

Figure 3.2: Top view of the surface turbulence setup. A sheet of laser light illuminates an area of sidelength 7 cm on the surface right below the high speed camera. Floating particles advected by turbulence in the tank scatter incident light which is captured by the camera. The movie is stored in a workstation whose output is later processed to construct the velocity fields.

3.2 EXPERIMENTAL SETUP.

The experimental setup is the same as discussed in section 2.3, but measurements are now made at the surface. Figure 3.2 sketches the top view of the setup (for a detailed discussion also see [18]). The tank of side length 1 m is filled with water to a height of 30 cm. A sheet of laser is generated by passing the beam through a cylindrical lens. Steady state turbulence is achieved by means of a pump (8 hp) that circulates water within the tank through a system of 36 rotating capped jets placed at the tank floor. This scheme of injection was chosen so as to minimize surface waves [33]. Hollow glass spheres of mean diameter 50 μm and specific gravity 0.25 are steadily injected from the bottom of the tank. Due to buoyancy the particles reach the surface and scatter the incident laser light which is captured by a high speed camera (Phantom v5.0) at a sampling rate of 400 frames per second. The camera covers a square area of sidelength 7 cm. Particles constantly leave the field of view, thereby necessitating steady seeding from the bottom in order to sample the steady state velocity fields at the surface. The spatial resolution set by the pixel size in the camera's charge coupled device (CCD) sensor is estimated to be 7 cm/1024 pixels $\simeq 70\mu$m. The camera's movie recording is broken into a series of TIFF images. Every $(n)^{th}$ and $(n+3)^{rd}$ image is passed through a particle tracking program [59] that correlates the image pair to obtain the x and y components of particle positions and velocities. Since every third image is chosen for velocity field construction, the effective time between images is $(1/400)$ s $\times$ 3 = 7.5 ms. The velocity resolution in this experiment is therefore of the order of 70 μm/7.5 ms $\simeq$ 1 cm/s. On average 16000 velocity vectors are recovered for velocity fields constructed from raw images. The eulerian and lagrangian parameters that characterize the turbulence in this experiment are given in Table 3.1.

Table 3.1: Eulerian and Lagrangian Turbulent quantities of interest measured in the experiment.

Parameter	Expression	Measured Value
Taylor Microscale λ (cm)	$\sqrt{\frac{u_{rms}^2}{\langle(\partial u_x/\partial x)^2\rangle}}$	0.3
Taylor Microscale Reynolds Number Re_λ	$\frac{u_{rms}\lambda}{\nu}$	85
Integral Scale l_0 (cm)	$1-\frac{1}{2}\frac{S_2(r)}{\langle u_L^2\rangle}$	1.3
Eulerian Large Eddy Turnover Time τ_0 (s)	$\frac{l_0}{u_{rms}}$	0.47
Lagrangian Correlation Time (Long.) $\tau_0^{\|\|}$ (s)	1 - $\frac{1}{2}\frac{D_2^{\|\|}(\tau)}{\langle u_{\|\|}^2\rangle}$	0.56
Lagrangian Correlation Time (Trans.) $\tau_0^{\perp}$ (s)	1 - $\frac{1}{2}\frac{D_2^{\perp}(\tau)}{\langle u_{\perp}^2\rangle}$	0.38
Dissipation Rate ε_{diss} (cm^2/s^3)	$10\nu\langle(\frac{\partial u_x}{\partial x})^2\rangle$	7.95
Kolmogorov Scale η (cm)	$(\frac{\nu^3}{\varepsilon_{diss}})^{1/4}$	0.02
RMS Velocity u_{rms} (cm/s)	$\sqrt{\langle u_L^2\rangle-\langle u_L\rangle^2}$	2.75
Compressibility C	$\frac{\langle(\vec{\nabla}\cdot\vec{v})^2\rangle}{\langle(\vec{\nabla}\vec{v})^2\rangle}$	0.53

3.3 MEASUREMENTS IN THE EULERIAN FRAME.

3.3.1 METHOD OF ANALYSIS.

The Eulerian structure functions (moments) are calculated directly from the experimental velocity fields. Each instantaneous velocity field is read into the moment calculation program separately. Taking each particle as the origin in the instantaneous snapshot of velocity field, two concentric circles of radii r and $(r+\Delta r)$ are considered such that the fractional area $(r/\Delta r)$ remains a constant. By trial and error, the smallest fractional area that provides statistical signficance is found to be 0.05. All particles within the concentric area are then considered for calculation of velocity differences with the particle at the origin for that particular r-value. This process is repeated for every particle in the instantaneous velocity field. Adequate care is taken not to double count particle pairs. All values of velocity differences are then written into a temporary memory location. The above process is then

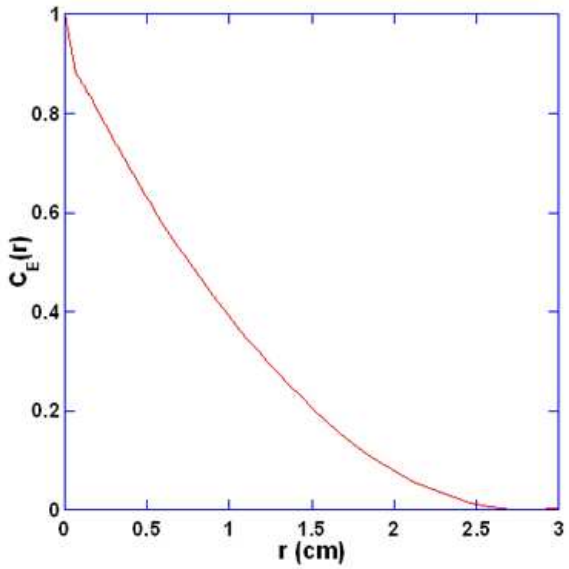

Figure 3.3: Correlation function of velocity differences in eulerian frame. It is calculated directly from the second-order structure function by taking $C_E(r) = 1 - (1/2)S_2(r)/\langle u_L^2 \rangle$. The area under this curve gives the integral scale of turbulence l_0 and is calculated to be 1.3 cm.

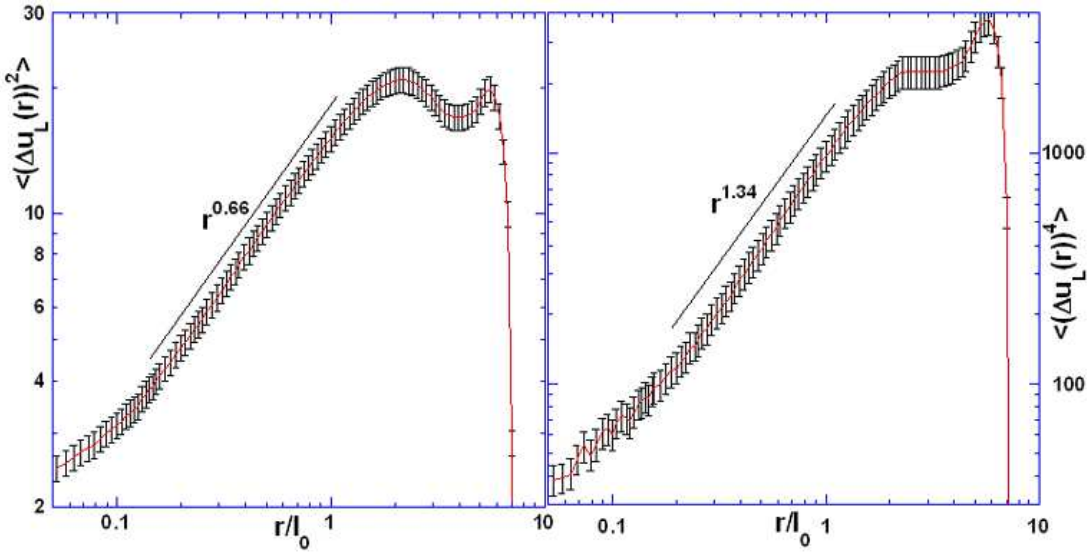

Figure 3.4: Eulerian structure functions $S_n(r) = \langle(\delta u_L(r))^n\rangle$ *vs.* r calculated for (a) $n = 2$, and (b) $n = 4$ at the surface. The spatial units have been normalized by the Integral scale $l_0 = 1.3$ cm. The statistical error, as denoted by error bars, is of the order of 5%.

repeated for nine time-uncorrelated velocity field snapshots. A global average is taken over all velocity differences obtained from the nine time-uncorrelated snapshots to obtain the eulerian moment at each r-value. On average about 10^5 particle pairs contribute to calculation of the eulerian moment at each r-value, providing very high statistical significance. Moments out to n = 12 are found to be reliable. However, here only the first four moments are considered. Analysis of temporal energy flux fluctuations is conducted in the same manner as discussed in section (2.4.2).

3.3.2 EULERIAN CORRELATION AND STRUCTURE FUNCTIONS.

The correlation function for spatial fluctuations in velocity differences is calculated directly from the eulerian second-order structure function by defining the normalized correlation function as $C_E(r) = 1 - \frac{1}{2}\frac{S_2(r)}{\langle u_L^2\rangle}$ and is shown in fig. 3.3. The area under this plot provides an experimental estimate of the integral scale of turbulence (l_0), calculated here to be 1.3 cm.

Shown in Fig. 3.4 are the second and fourth-order structure functions calculated in the eulerian frame. They exhibit Kolmogorov scaling expected of structure functions in incompressible turbulence $S_n(r) \sim (\bar{\varepsilon} r)^{n/3}$. The structure functions are plotted in dimensionless units r/l_0. As shown in the figure, the plots exhibit a power-law scaling of $r^{(0.66\pm0.02)}$ for second-order structure function and $r^{(1.34\pm0.03)}$ for the fourth-order structure function over a little more than a decade. This scaling has been previously reported in [18]. There the authors also showed effects due to intermittency were higher at the surface, which show up for higher-order structure functions. These results are therefore not new. They have only been calculated here to ensure agreement of the present data set with previous measurements.

One of the main quantities of interest in this experimental study is the third-order eulerian structure function since K41 provides an exact result for this quantity in case of incompressible turbulence. It is plotted in Fig. 3.5 for both the incompressible bulk and compressible surface turbulence data sets as a function of dimensionless length r/l_0 (the normalization is achieved by the bulk and surface integral scales respectively). In fact the $S_3(r)$ calculated at the surface is even better than one obtained from the incompressible bulk flow. The incompressible bulk data set is the one applied for analysis of energy flux fluctuations in Chapter 2. In addition, fig. 3.6 shows the third-order structure functions for incompressible bulk (red) and compressible surface (green) turbulence as obtained from direct numerical simulations under flow conditions close to those in the present experiment. There the x-axis is in dimensionless spatial units where the distance r has been normalized by the integral scale of bulk turbulence and y-axis plots $S_3(r)$. The simulations were performed by J. Schumacher, J. Davoudi and B. Eckhardt, Philipps Universität, Marburg Germany. In the interval $0 < r/l_0 < 1.4$ good qualitiative agreement is observed between the experimental results plotted in Fig. 3.5 and simulation results plotted in Fig. 3.6. Given prior knowledge of the eulerian structure functions exhibiting Kolmogorov scaling, the scaling of third-order structure function linearly in r was expected on dimensional grounds. However, the compressible nature of turbulence at the surface leaves open the question of whether $S_3(r)$ would take on a positive or negative sign since $S_3(r) \sim +r$ would be dimensionally as permissible as $S_3(r) \sim -r$. It is therefore noteworthy that $S_3(r)$ follows the same sign as expected from four-fifth law.

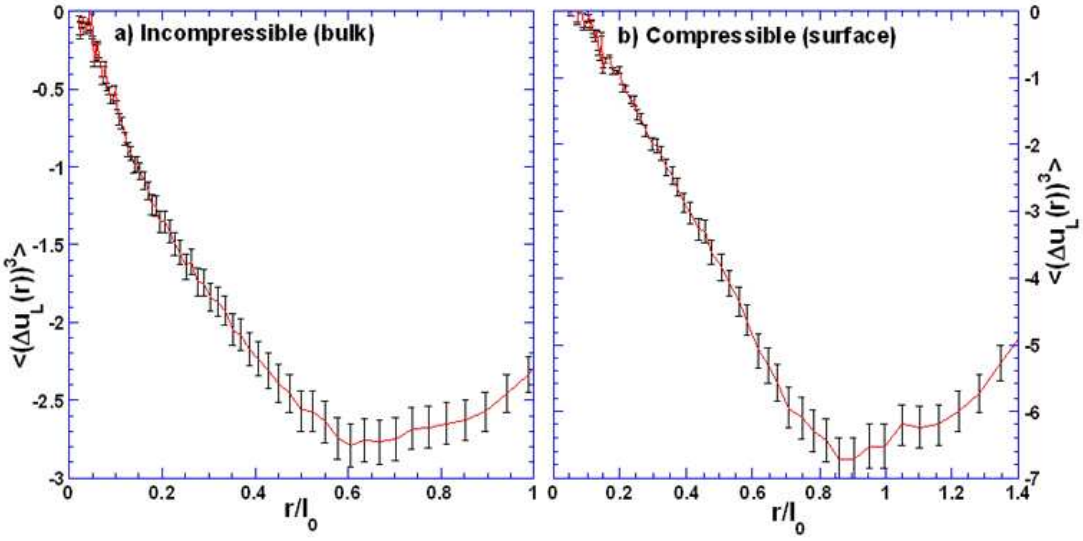

Figure 3.5: The third-order eulerian structure function $S_3(r) = \langle(\Delta u_L(r))^3\rangle$ *vs.* r calculated for (a) the incompressible bulk, and (b) the compressible surface data. The spatial units have been normalized by the respective integral scales l_0 for the incompressible bulk ($l_0 = 3.5$ cm) and compressible surface ($l_0 = 1.3$ cm) data. The statistical error as denoted by the error bars is about 5%.

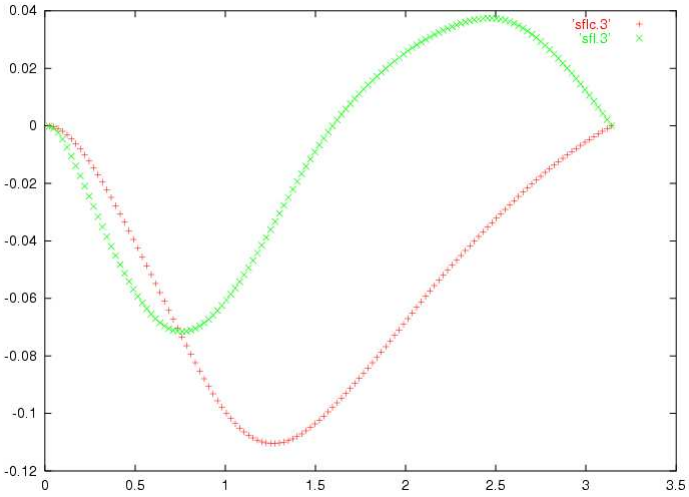

Figure 3.6: The third-order eulerian structure function $S_3(r) = \langle(\delta u_L(r))^3\rangle$ *vs.* r as obtained from direct numerical simulations for surface (green) and the incompressible bulk (red). The length r on the horizontal axis is normalized by the bulk integral scale. (*Courtesy of J. Schumacher, Technische Universität, Ilmenau, and J. Davoudi, Philipps Universität Marburg, Germany*).

There is no reason to expect Kolmogorov scaling for Eulerian structure functions at the surface. In fact arguments against applicability of the Kolmogorov theory for surface flow far outweigh the arguments in favour. The Kolmogorov theory is predicated upon assumptions of homogeneity, isotropy and incompressibility of the turbulent flow. Since surface turbulence is strongly compressible, there exists no basis for application of the Kolmogorov theory. In addition, the surface is intricately coupled with its underlying incompressible bulk, and exchanges energy and enstropy simultaneously at all spatial scales with it. Therefore one cannot expect conservation of energy at the surface even in the absence of viscosity ($\nu \rightarrow 0$). For the same reason one may also not expect an inertial sub-range at the surface as spatial and temporal correlations ought to be destroyed due to simultaneous eddy-exchange between the surface and bulk. Yet as seen in Fig. 3.5, the third-order structure function clearly scales linearly with r suggesting that it upholds the four-fifth law at the surface. It is understood that the existence of an energy cascade requires agreement with the four-fifth law (for incompressible flows). In the converse case does agreement with four-fifth law automatically predicate the existence of an energy cascade? The author is unsure of this. It is not as if compressible flows do not exhibit a cascade. One knows that the Burger's equation admits compressible effects and does have have an energy cascade [35]. There too the third-order structure function scales linearly with r and is called the "twelve law" ($S_3(x) = -12x$).

The PDF of energy flux $\varepsilon(r,t)$ was calculated for incompressible turbulence in Chapter 2. The skewness in that PDF is usually considered an indication of the directional preference of energy transfer in incompressible turbulence towards small spatial scales (private communication with Charles Meneveau). Any observable skewness in the PDF of the quantity analogous to energy flux at the surface would therefore be helpful in learning further about the directionality of energy transfer, if any, at the surface.

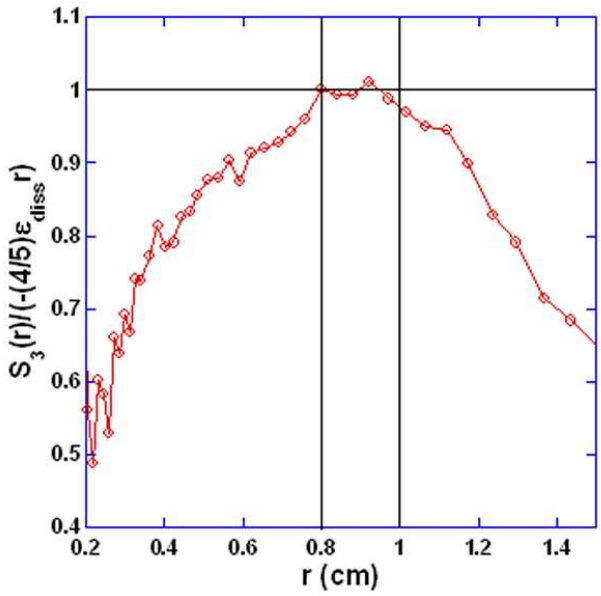

Figure 3.7: The ratio $\frac{S_3(r,t)}{[-(4/5)\varepsilon_{diss}r]}$ *vs.* r shows a limited region (0.8 cm $\geq$ r $\geq$ 1.0 cm) where the plot has zero slope.

3.3.3 TEMPORAL FLUCTUATIONS IN TURBULENT ENERGY FLUX AT THE SURFACE.

Assuming the four-fifth law does indeed hold at the surface, one can proceed with the analysis of energy flux fluctuations discussed in section (2.4.2) for the surface turbulence data. The range of spatial scales where the measurements may be reliable are first ascertained by plotting the ratio $S_3(r)/[-\frac{4}{5}\varepsilon_{diss}r]$ *vs.* r. For incompressible turbulence this plot is a horizontal line of zero slope at a value of unity, and is shown here for the surface data in Fig. 3.7. In fact a comparison with Fig. 2.4 shows agreement of the ratio with the expected value of unity at the surface is even better than for the bulk. A limited range of spatial scales between $r = 0.8$ cm and $r = 1$ cm are found to agree with this requirement. The spatial scale $r = 0.9$ cm is chosen for analyzing the energy flux fluctuations. Defining $\varepsilon(r,t) = \frac{S_3(r,t)}{-(4/5)r}$, a time-trace of $\varepsilon(r,t)$ is obtained from the third-order structure function measured for each instant of the collected data. This time-trace is shown in the inset to Fig. 3.8. The main

figure shows the probability distribution of the flux. The PDF exhibits a marked skewness towards positive values of $\varepsilon(r,t)$ similar to the plots (see Fig. 2.6) obtained for incompressible data. This suggests there may indeed be some merit to the notion of an energy cascade at the surface. If the second-order lagrangian structure function also shows linear scaling in τ, one may have a strong case to argue the existence of an energy cascade at the surface. Results from lagrangian analysis are discussing in the next section.

3.4 MEASUREMENTS IN THE LAGRANGIAN FRAME.

3.4.1 METHOD OF ANALYSIS.

For all analysis in the lagrangian frame, the experimentally obtained velocity fields are seeded with fictitious (surrogate) particles via computer programming. At $t = 0$, the 1024 x 1024 pixel grid of the velocity field is decorated with a uniform array of surrogate particles 8 pixels apart, providing $128^2 = 16384$ surrogate particles. Evolution of this initially uniform particle distribution is dictated by the experimentally obtained velocity fields. The particles are tracked by the program instant by instant in the lagrangian frame. Though some particles leave the field of view during the evolution time, they are tracked as long as they remain in it. For every surrogate particle that leaves the field, a new particle is introduced at a random spatial point within it, thereby creating a new lagrangian trajectory. Real particles are substituted with surrogates in order to achieve particle tracking in the lagrangian frame. A total of 120000 lagrangian trajectories were evolved throughout the 5 s duration. Some of the trajectories were discarded as they left the field almost immediately. About 104000 trajectories were considered for the final analysis of lagrangian structure functions.

3.4.2 LAGRANGIAN CORRELATION AND STRUCTURE FUNCTIONS.

Kolmogorov theory sets a preferential component (longitudinal) along which to measure velocity differences in the eulerian frame. Since it is not clear if a similar preferential component exists in the lagrangian frame, both components of lagrangian velocity differences are ana-

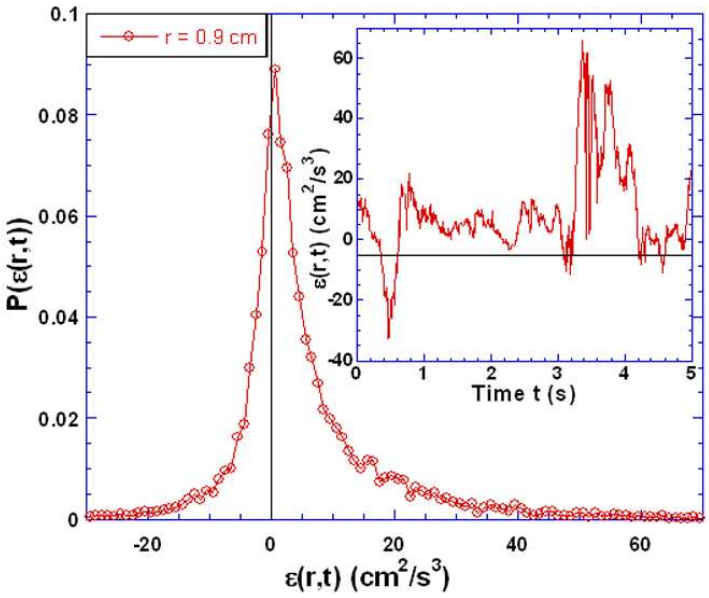

Figure 3.8: The PDF of energy flux defined as $\varepsilon(r,t) = S_3(r,t)/(-\frac{4}{5}r)$ plotted for $r = 0.9$ cm and subdomain size of side length $L = 1.75$ cm. Inset shows the time trace of energy flux ε.

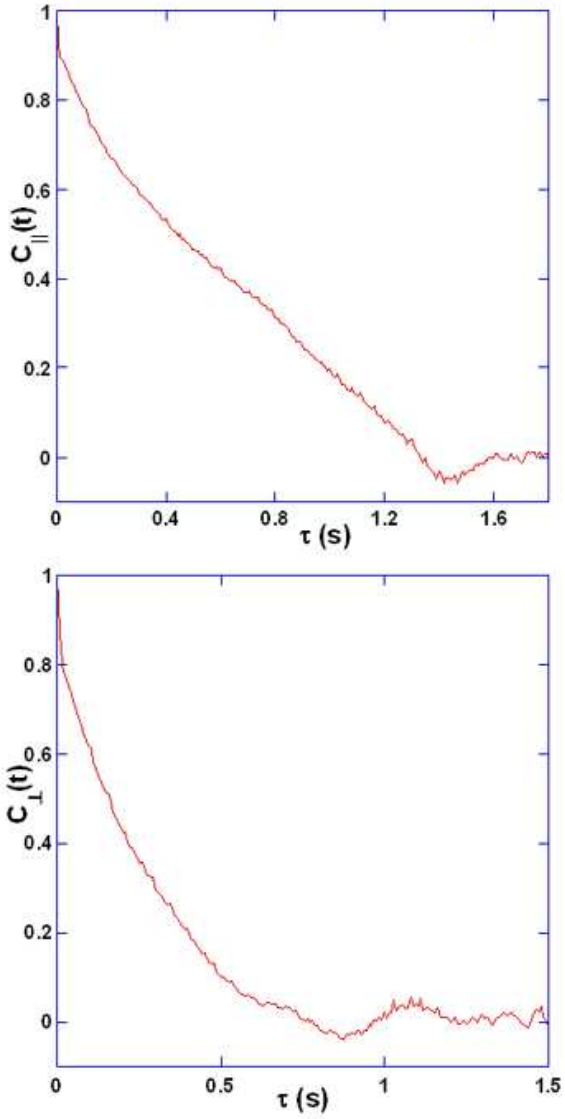

Figure 3.9: The lagrangian correlation functions along the longitudinal $C_{||}(\tau) = 1 - (1/2)D_2^{||}(\tau)/\langle u_{||}^2 \rangle$ and transverse $C_{\perp}(\tau) = 1 - (1/2)D_2^{\perp}(\tau)/\langle u_{\perp}^2 \rangle$ directions. The area under these curves gives the lagrangian correlation time and is calculated to be 0.56 s along the longitudinal direction and 0.38 s along the transverse direction.

lyzed. In any case, any component ought to be suitable for lagrangian measurements since one expects that temporal increments of velocity are equally probably along all directions. Figure 3.9 shows the lagrangian correlation function of velocity differences along the longitudinal ($||$) and transverse ($\perp$) directions. The correlation time is calculated to be about 0.56 s for the longitudinal component and 0.38 s for the transverse component. As in the Eulerian case, here too the correlation functions were calculated from their respective lagrangian second-order structure functions by defining the correlation function as $C(\tau) = 1 - \frac{1}{2}\frac{D_2(\tau)}{\langle u^2 \rangle}$.

As may be observed in Fig. 3.9, the longitudinal correlation function decays linearly after an initial intervale ~ 0.2 s. No linear decay is observed along the transverse direction. This point is noteworthy given that the lagrangian correlation function in **incompressible** turbulence is expected to decay linearly (see [47] pages 547 - 548 for theoretical arguments and underlying assumptions). Experimental evidence for linear decay of lagrangian velocity fluctuations is however poor. In [49] Mordant et. al. reported exponential decay for the velocity autocorrelation function for incompressible turbulence experiments in the lagrangian frame. The expectation of a linear decay is also intuitively understood if one plugs in the expected scaling for $D_2(\tau)$ in $C(\tau)$. Then $C(\tau) = 1 - \frac{1}{2}\frac{D_2(\tau)}{\langle u^2 \rangle} = 1 - \frac{1}{2}\frac{C_0 \bar{\varepsilon} \tau}{\langle u^2 \rangle}$.

Figure 3.10 plots the second important result of this study, the lagrangian second-order structure function for both longitudinal and transverse components in linear scale. The scaling here is consistent with the decay form observed for the corresponding correlation functions in fig. 3.9. The longitudinal second-order structure function scales linearly as already seen from its correlation function, however the linear scaling occurs only at times $\tau \geq \tau_0^{||}$. The transverse structure function on the other hand shows no such scaling. The linear scaling in τ is expected for earlier times $\tau \leq \tau_0$ in both components.

If the second-order structure function is plotted in log-log scale, one sees a clear power-law scaling pattern at early times $\tau_\eta \ll \tau \leq \tau_0$ for both components over more than a decade. Figure 3.11 (a) and (b) show the plots in log-log scale for both components. $D_2(\tau)$ scales as $\tau^{1/2}$ for both components of lagrangian velocity differences at the surface. It does not scale linearly as one expects in incompressible turbulence. Is this scaling behavior coming from the compressible effects that exist at the surface? One is not sure. The power-law exponent close to 1/2 is discussed nowhere in literature to the author's best knowledge. The absence

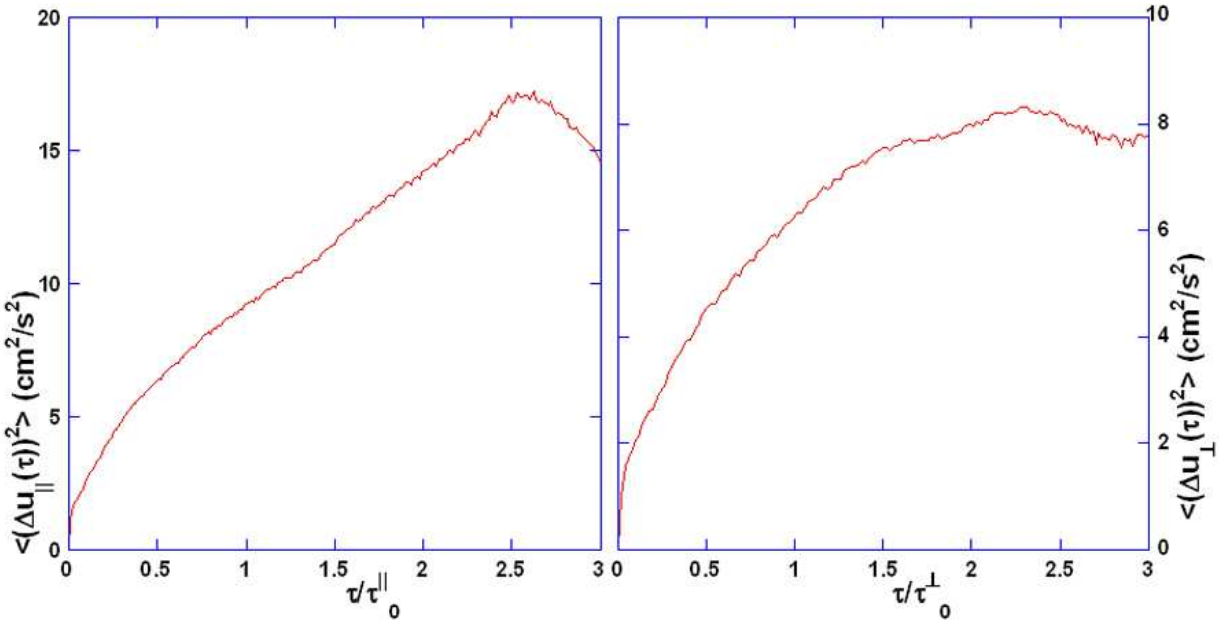

Figure 3.10: The lagrangian second order structure function for longitudinal (||) and transverse ($\perp$) components, in linear scale. One sees a linear scaling for the longitudinal component only beyond τ greater than the longitudinal correlation time of 0.56 s. For the transverse case no linear scaling is apparent.

of a theory to attack the compressible surface phenomena makes it even more difficult to make simple estimates of what scaling ought to be expected for free surface turbulence.

The possibility exists that one may be able to calculate scaling exponents for higher-order structure functions and extract a dimensional formula for lagrangian velocity statistics. Such an expectation is however fraught with many difficulties as will be discussed shortly. Figure 3.11 (c) and (d) plots the lagrangian fourth-order structure function. No scaling is observed for the longitudinal case. The transverse component however reveals a small region that scales as $\tau^{1.34}$. No scaling regime is observed for the sixth-order structure function (not shown here). The odd-moments of lagrangian velocity differences (not shown here) did not reveal any scaling.

There are severe interpretational difficulties involved in a dimensional approach to the scaling exponents in this analysis.

1) Previous studies [18] have revealed intermittency effects are higher at the surface as compared to the incompressible bulk. In addition experiments [49, 75, 48, 76] also show lagrangian statistics are more intermittent than eulerian statistics in incompressible turbulence. The present study is therefore complicated by compounded effects of intermittency arising from two sources. As a result one is assured of scaling, if any present, would be highly anomalous for free-surface turbulence. In anycase, anomalous scaling due to intermittency is observed for higher-order statistics. If one naively hopes the same to hold true for present analysis, the scaling observed for lagrangian second-order structure function ought to be devoid of effects contributed due to intermittency.

2) In case of incompressible turbulence, the entire study of anomalous exponents came about due to failure of Kolmogorov theory for higher-order structure functions. The difference between expected and observed exponents is attributed to intermittency. In the absence of a suitable theoretical framework for free surface turbulence, there exist no expected scaling exponents. It is therefore impossible to dissociate intermittency driven anomalous scaling from the expected dimensional form.

3) Another source of complication is the fact that odd-order structure functions are expected to be zero in lagrangian measurements (at least in the incompressible case). The probability of observing $\Delta u(\tau)$ and $-\Delta u(\tau)$ is the same in lagrangian frame. This is at-

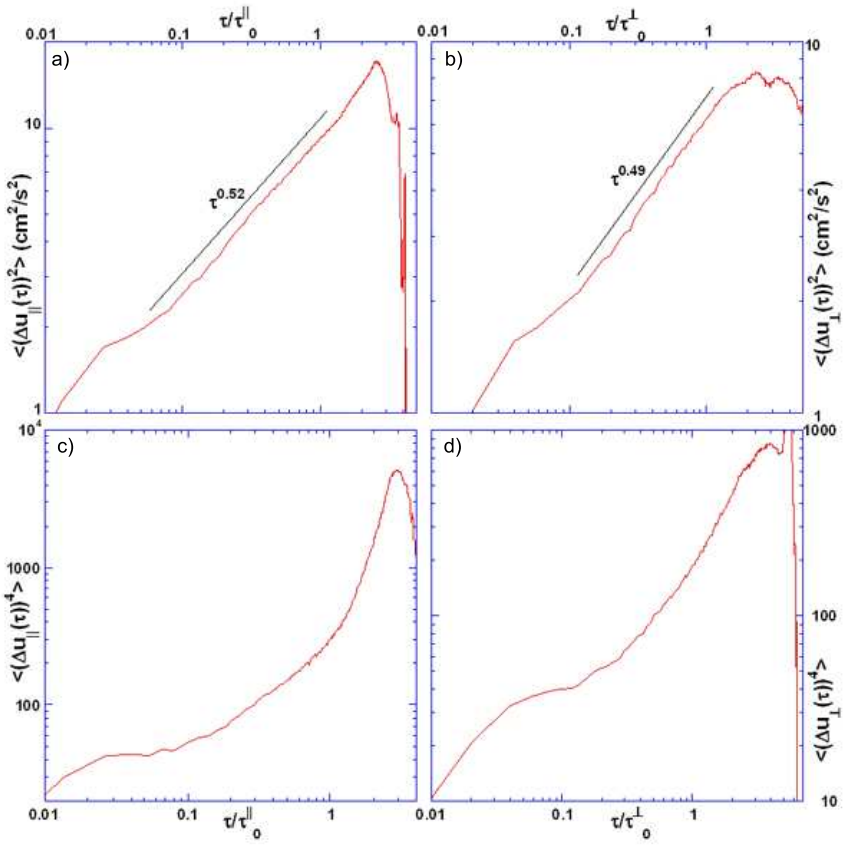

Figure 3.11: The second and fourth order structure functions for both longitudinal and transverse components of lagrangian velocity differences plotted in log-log scale.

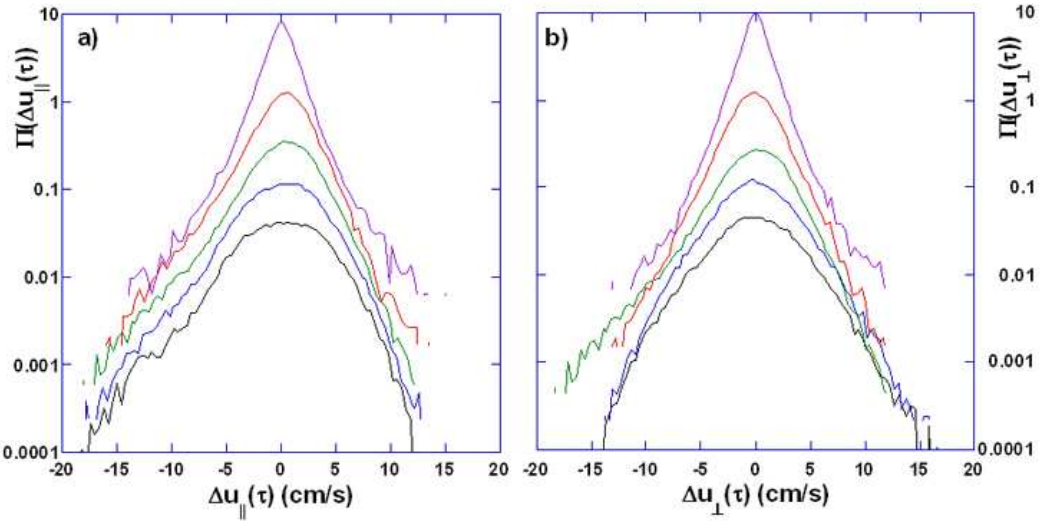

Figure 3.12: The PDFs of lagrangian velocity differences for different times τ, vertically displaced for sake of clarity with time τ increasing from top to bottom. (a) $\tau/\tau_0^{||} = 0.056, 0.28, 0.56, 0.83,$ and $1.11.$ for longitudinal component and (b) $\tau/\tau_0^{\perp} = 0.08, 0.4, 0.8, 1.18,$ and 1.58 for the transverse component. In both cases the PDFs do not approach a gaussian profile with increasing τ as was expected. Instead there is a marked increase in skewness with increasing τ.

tributed to the fact that the probability of a particle increasing its velocity is the same along all directions in the lagrangian frame (see [47] page 360). Nonetheless it is worth mentioning that H. Xu et. al. [75] do report measurements for odd-moments of lagrangian velocity differences suggesting that they are non-zero even in incompressible turbulence. In the present case of surface turbulence the PDFs of lagrangian velocity differences plotted for various dimensionless times τ/τ_0 in Fig. 3.12 for surface measurements reveal that the probability distributions are only skew symmetric for small times. As τ/τ_0 increases, a marked skewness develops for both longitudinal and transverse components. This is a clear indication that odd-moments for surface lagrangian measurements are not zero as in case of incompressible turbulence. When the third and fifth-order structure functions were plotted no scaling pattern was observable. Events contributing to odd-moments of a distribution can take both positive and negative values, thus demanding many events in order to achieve statistical significance for the odd-moments. The present dataset does not provide enough events to achieve such statistical significance for the odd-order structure functions.

4) A further complication arises from the PDFs plotted in Fig. 3.12. At $\tau \simeq \tau_0$ the velocities become decorrelated. This translates to the expectation that the PDF of velocity differences should approach a gaussian form (barring finite effects of large deviation theorem) as τ increases. This is clearly the case for incompressible lagrangian measurements [49]. The PDFs in Fig. 3.12 do not approach a gaussian suggesting there exists a characteristic time of turbulence greater than τ_0 for surface flows. No analog to such argument exists in the theory of incompressible turbulence.

3.5 CONCLUSION.

In summary, the velocity statistics for compressible turbulence are studied in both the eulerian and lagrangian frames. In accord with previous studies, Kolmogorov scaling is observed for eulerian structure functions. The third-order eulerian structure function is measured for the first time and is found to agree very well with the Kolmogorov four-fifth law, thus suggesting the possibility of an energy cascade at the surface despite violation of the in-

compressibility requirement. A repetition of the energy flux analysis discussed in Chapter 2 reveals a positive skewness in the PDF of scale dependant energy flux $\varepsilon(r,t)$ further strengthening the possibility for a cascade process.

Analysis conducted on the same dataset in the lagrangian frame reveals that the second-order structure function does not scale linearly in time τ as predicted for incompressible turbulence. Instead a power-law scaling with an exponent close to 1/2 is observed. This leads to a scaling mismatch between eulerian and lagrangian observations.

Higher order even and odd structure functions reveal little information on scaling exponents. Intermittency is known to be higher at the surface, in addition to higher intermittency reported for lagrangian measurements in incompressible flows. It is possible that both conditions compound intermittency effects for lagrangian analysis at the surface thus leading to highly anomalous exponents for higher order structure functions. The absence of a suitable theory prevents one from making any prediction on the degree to which exponents deviate. Though odd-order structure functions are expected to be zero in the lagrangian frame, the skewness observed at long times in PDFs of lagrangian velocity differences suggests such may not be the case for surface flows. In addition the absence of a gaussian form for PDFs at long times begs one to ask if there exists a characteristic time longer than the large eddy turnover time for the surface. The statistics collected for this analysis prove insufficient for calculation of the odd-moments of lagrangian velocity differences.

This study remains inconclusive on whether a cascade process exists at the surface, and on the scaling patterns one may expect for lagrangian velocity differences. It is felt that data collected over a longer duration leading to many more lagrangian trajectories may help improve the statistics significantly. In case of incompressible turbulence, the failure of Kolmogorov theory paved way for a systematic analysis of anomalous exponents culminating in the theory of long-lived structures or zero-modes [27]. It is felt that instead of looking for dimensional arguments in lagrangian structure functions, theoretical guidance rooted in the zero-modes approach [27] for compressible turbulence at the free surface would prove beneficial for experimentalists to proceed further with a systematic analysis.

4.0 ENTROPY PRODUCTION RATE IN COMPRESSIBLE TURBULENCE.

4.1 INTRODUCTION.

In nature one often finds the behavior of macroscopic systems is irreversible. For instance, an ink drop introduced in a container of clear water disperses over time until ink is homogeneously distributed throughout the container's fluid. One never observes the reverse instance of dispersed ink concentrating itself at a point [41]. This irreversible aspect of nature is captured by the statistical notion of entropy. Entropy is defined in such a manner that it can either remain constant or increase with time for an isolated macroscopic system. This is the essence of the second law of thermodynamics. A constant entropy coincides with the equilibrium condition whereas a strict increase in entropy is achieved by any one of two means. The removal of a constraint for a system in thermal equilibrium requires it to relax into its new equilibrium state leading to an increase in entropy. Alternatively, injecting energy into a system in equilibrium kicks it into a non-equilibrium state. The system is then required to dissipate this energy as heat, again leading to an increase in entropy. When energy is injected into the system at a constant rate it also dissipates energy into heat at the same constant rate (on the average). This is referred to as the condition of non-equilibrium steady state. In the steady state the system naturally produces entropy at a constant rate.

A serious problem however emerges in the definition of entropy for systems driven far from thermal equilibrium. Such systems exhibit wild fluctuations with long spatial and temporal correlations in measured parameters, thus making it difficult to characterize temperature and entropy for non-equilibrium processes. Attempts to define a dynamical or effective temperature in such systems have so far met with little success. The correlations also

introduce a temporal dependence into statistical quantities, suggesting that the entropy rate rather than entropy itself is a more meaningful quantity for the nonequilibrium condition. More importantly, there presently exists no official definition of entropy for nonequilibrium systems (private communication with G. Gallavotti).

In recent theoretical work Falkovich and Fouxon [26, 25] rigorously derive an expression for the entropy production rate $\dot{S}$ for a system in the non-equilibrium steady state (see Appendix A for the derivation). The theory rests on the assumption that the system is highly chaotic and admits distributions of the Sinai-Ruelle-Bowen (SRB) type [25]. The SRB distributions are characterized by a smooth distribution of points (particles in real space or phase points in higher dimensional phase space) along the unstable manifold and a fractal distribution along transverse directions. Under such assumptions, they show that the entropy production rate equals the negative of the time integral of the temporal correlation function of velocity divergence in the lagrangian frame of reference. In addition, they also show that $\dot{S}$ equals the sum of the system's Lyapunov exponents. The definition of entropy $S(t)$ is dimensionless and translates to a statement regarding probabilities. This definition is therefore applicable to density of points in phase space or the concentration of particles in a compressible flow in real space.

The experiments discussed here are conducted in configuration (real) space for a system of particles that float on the surface of water maintained in a turbulent steady state. This system of floaters forms a strongly compressible system even at low Mach numbers. Do note that under the definition adopted here, the entropy S(t) represents the disorder in the system and is not related to thermodynamic entropy.

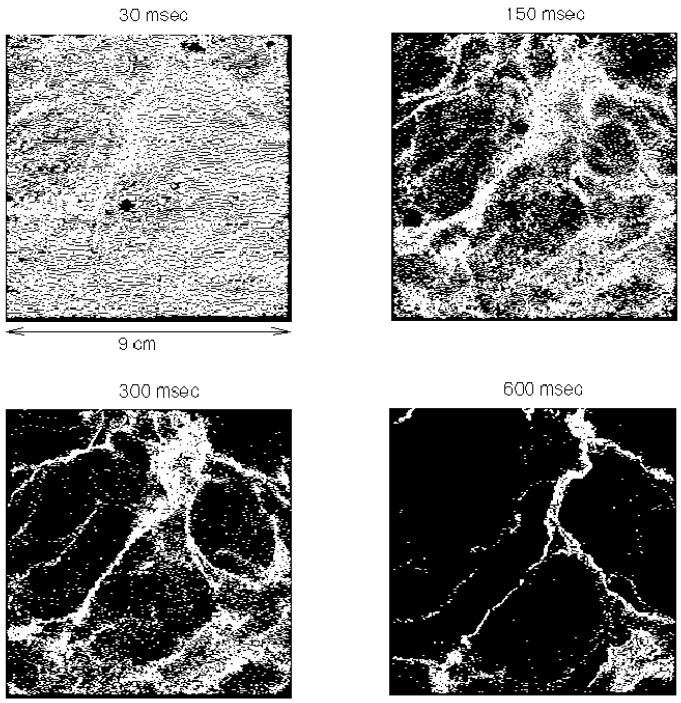

Figure 4.1: A system of fictitious (surrogate) particles is introduced on the experimental velocity fields at $t = 0$. The distribution of particles is homogeneous to start with. However the particles quickly flee regions of fluid up-wellings and cluster into thin ribbon like structures around fluid down-wellings as time progresses. The evolution of clusters is shown for four snapshots in time as they evolve from a nearly homogeneous distribution at $t = 30$ ms towards an inhomogeneous distribution through $t = 150$ ms and 300 ms. The experiment is almost over at $t = 600$ ms by which time particles have almost completely clustered into ribbon like structures.

4.2 EXPERIMENT.

4.2.1 APPLICATION OF THE THEORY TO COMPRESSIBLE TURBULENCE ON A FREE SURFACE.

The floaters sample the velocity field at the surface of water, which is incompressible. For them an initially uniformly distributed array of particles will subsequently tend to cluster under influence of the underlying turbulent fluid motion, as shown in Fig. 4.1, thus reducing their total entropy, defined as:

$$S(t) = -\int d\mathbf{r}\ n(\mathbf{r},t) \ln\ n(\mathbf{r},t). \tag{4.1}$$

Here $n(\mathbf{r},t)$ is the local concentration of particles on the surface. The integral is over an area spanned by an overhead camera that records the motion of floaters. One may regard the water beneath the floaters as providing an energy reservoir or thermostat which exchanges energy (and vorticity) with the floaters, and perhaps defines a dynamical temperature of the system. The dimensions of the water tank are large compared to the largest scales of turbulent flow. To understand the statistical mechanics of floaters, one need not be concerned with details of the turbulent flow that drives them [18, 5].

Falkovich and Fouxon [26] (FF) have shown that the entropy production rate $\dot{S}$ of compressible systems, like the floating particles in this experiment, is nonzero. The floaters "live" on the surface and thus have a two-dimensional velocity divergence $\omega(\mathbf{r},t) \equiv \vec{\nabla}_2 \cdot \vec{v}(\mathbf{r},t)$ (also see chapter 3). The fluid, being incompressible everywhere, including the surface, tracer particles (specific gravity 0.25) obey the equation $\vec{\nabla}_2 \cdot \vec{v} = \partial_x v_x + \partial_y v_y = -\partial_z v_z \neq 0$. The finite compressibility of the floating particle system is the origin of the nonzero value of $\dot{S}$.

This quantity can be written as the sum of two terms [26]:

$$\dot{S} = \int_V d\mathbf{r}\ n(\mathbf{r},t)\omega(\mathbf{r},t) + \int_{\partial V} n(\mathbf{r},t) \ln\ n(\mathbf{r},t)\mathbf{v}.d\mathbf{S} \tag{4.2}$$

The first term is an integral over the area (area term) spanned by a camera which records the motion of floaters; the second term is a line integral around the periphery of designated particles (boundary term) that escape from the camera's field of view. Eq. (4.2) is derived

from Eq. (4.1) above by applying the condition for mass conservation which translates to conservation of particles in this experiment ($\partial_t n(\mathbf{r},t) + \nabla_2 \cdot (n(\mathbf{r},t)\mathbf{v}(\mathbf{r},t)) = 0$). Despite the existence of viscous dissipation in the incompressible bulk, the entropy rate in Eq. 4.2 is zero there. $\dot{S}$ is therefore not a quantifier of thermodynamic entropy rate, and hence not related to the heat flux in the system. FF assume that the boundary term is zero and work exclusively with the area term. Under the assumption that the system admits SRB statistics (by equating the long-time probability measure $\mu_{lim\to\infty} = \mu_{SRB}$, see [25] for the derivation), FF show that the first term on the right is the integral of the temporal correlation function of the lagrangian velocity divergence with a negative prefactor.

$$\dot{S} = -\int d\tau \ \langle \omega(\mathbf{r},t)\omega(\mathbf{r},t+\tau)\rangle. \tag{4.3}$$

Here $\mathbf{r}$ is the starting point of the trajectories, and $\langle ... \rangle$ represent an average over both t and $\mathbf{r}$. Reported here are measurements of both the area and boundary term contributions to $\dot{S}$, a quantity that becomes time-independent after an initial transient period.

One can define a dimensionless compressibility $C = \frac{\langle(\vec{\nabla}_2\cdot\vec{v})^2\rangle}{\langle(\vec{\nabla}_2\vec{v})^2\rangle}$ [18], which lies between 0 and 1 for an isotropic system. Previous experiments and numerical studies [18] have consistently measured $C = 0.5$ at the surface, thus making the system of floaters a strongly compressible one.

4.2.2 SETUP

The experimental system is a tank of water 1 m x 1 m in lateral dimensions, filled to a depth of 30 cm and maintained in a turbulent steady state. The experimental setup is discussed in detail in [18]. Turbulence is generated by an 8 hp pump that circulates water in the tank via an array of 36 capped jets that rotate like lawn sprinklers on the tank floor. The points of turbulent injection are therefore far removed from the surface where measurements are made. The injection scheme was chosen to minimize the amplitude of waves on the surface [33]. Hollow glass spheres of mean diameter 50 μm and specific gravity 0.25 follow the local surface flow. A beam from a diode-pumped laser (5.5 W) is passed through a cylindrical lens to generate a sheet of light that illuminates the surface. Light

Table 4.1: Parameters of compressible turbulence measured at the surface.

Parameter	Expression	Measured value
Taylor microscale λ (cm)	$\sqrt{\frac{v_{rms}^2}{\langle(\partial v_x/\partial x)^2\rangle}}$	0.3
Re_λ	$\frac{v_{rms}\lambda}{\nu}$	93
Integral Scale l_0 (cm)	$\int dr \frac{\langle v_{\|\|}(x+r)v_{\|\|}(x)\rangle}{\langle(v_{\|\|}(x))^2\rangle}$	1.2
Dissipation Rate ε_{diss} (cm^2/s^3)	$10\nu\langle(\frac{\partial v_x}{\partial x})^2\rangle$	10.7
Kolmogorov Scale η (cm)	$\eta = (\frac{\nu^3}{\varepsilon})^{1/4}$	0.02
Large Eddy Turnover Time τ_0 (s)	$\tau_0 = \frac{l_0}{v_{rms}}$	0.54
RMS Velocity v_{rms} (cm/s)	$v_{rms} = \sqrt{\langle v_{\|\|}^2\rangle - \langle v_{\|\|}\rangle^2}$	2.6

scattered by the particles is captured by a high speed camera (Phantom v5.0) that records particle positions and velocities at 100 frames per second. Steady state flow measurements are achieved by constantly seeding floaters from the bottom of the tank to compensate for those that are lost from the camera's field of view. The computer-stored record is broken up into a series of images that are fed into a particle tracking program [59] in consecutive pairs to obtain the experimental steady-state flow velocity fields. A total of 2040 instantaneous velocity fields spanning a duration of 20 s are obtained. There are on the average 25000 velocity vectors in each velocity field, providing reliable spatial resolution over a square area of side length L = 9.3 cm. Parameters that characterize turbulence on the surface are listed in Table 4.1.

For the analysis discussed below, the experimentally obtained velocity fields are seeded with fictitious (surrogate) particles via computer programming. At $t = 0$, the 1024 x 1024 pixel grid of the velocity field is decorated with a uniform array of surrogate particles 6 pixels apart, providing $170^2 = 28900$ surrogate particles. Evolution of this initially uniform particle distribution is dictated by the experimentally obtained velocity fields. The particles are tracked by the program instant by instant in the lagrangian frame. Though some particles leave the field of view during the evolution time, they are tracked as long as they remain in the field of view. Essential to the theory of FF is the requirement that the number of

particles in the system be conserved. Hence for every surrogate particle that leaves the field of view, a new particle is introduced at a random spatial point within it, thereby representing a new lagrangian trajectory.

The focus of these experiments is on the rate of entropy production at times t large compared to the turnover time of largest eddies, estimated to be 0.54 s. The 20 s time record is broken up into 20 time-uncorrelated data sets of 1 s duration. The surrogate particles are tracked and the two terms of Eq. (4.2) measured for each data set and averaged over the 20 sets. Figure 4.1 shows the time evolution of one of these sets. Surrogate particles are used for entropy rate measurements since they allow an initial periodic placement which is not possible with real particles. In addition the surrogates also permit particle tracking in the lagrangian frame of reference. Lagrangian tracking of real particles is beyond the experimental capability of the current scheme.

4.3 ANALYSIS AND RESULTS.

Before examining the two terms in Eq.(4.2), it is of interest to examine time dependence of the entropy itself. Each instantaneous snapshot is divided into two-dimensional bins (cells) of side length 8 pixels. The particle concentration $n_i(t)$ is the number of particles in the i^{th} cell divided by the total number of particles in the field of view at time t. The local entropy is calculated for each cell i and the total instantaneous entropy as expressed in Eq. (4.1) is obtained from an average over all cells $S(t) = -\sum_{i=1}^{N} n_i(t) \ln n_i(t)$ in a given snapshot. The entropy $S(t)$, defined by Eq. (4.1), is an intensive quantity since $\sum_{i=1}^{N} n_i = 1$. Here N is the total number of cells in the field of view.

Figure 4.2 shows the time evolution of $S(t)$ over an interval of 1 s. The curve is an ensemble average of the 20 data sets measured at each instant of time t. Observe that $S(t)$ from Eq. (4.1) decreases monotonically through this time interval, implying that particle clustering increases with time. This accords with the visual observations of clustering tracked over 0.6 s in Fig. 4.1. The ensemble of $S(t)$ measurements is not large enough to completely average out its temporal fluctuations, making it impossible to extract its derivative. That

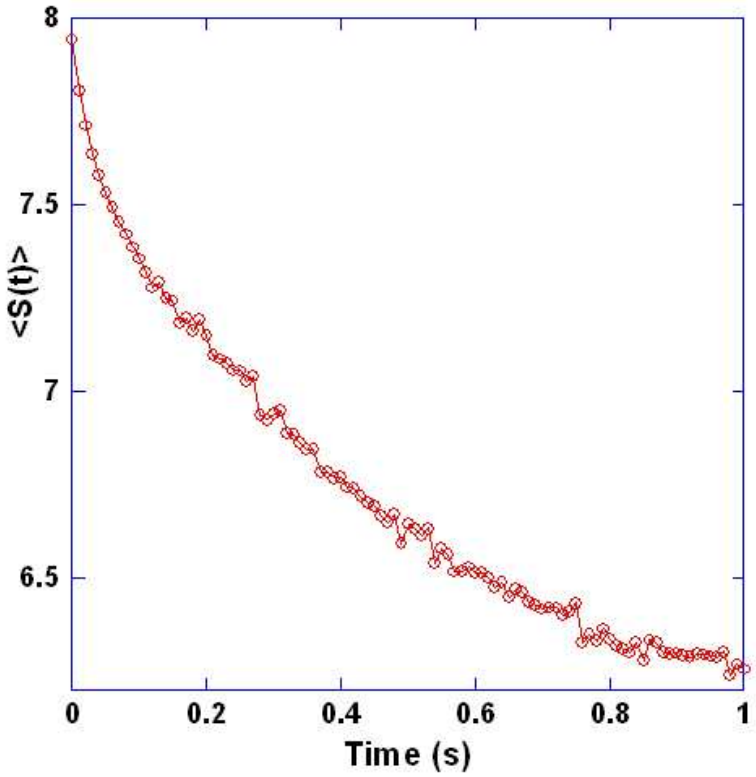

Figure 4.2: The measured entropy $S(t)$. The angular brackets around $S(t)$ denote an ensemble average over the 20 time-uncorrelated sets. Note the quantity shows monotonic decrease in time arising from the clustering of particles at the surface as observed in Fig. 4.1.

function is best obtained using Eq. (4.2).

The velocity divergence field $\omega(\mathbf{r}, t)$ is obtained by taking component-wise spatial derivative of the velocity fields at each instant. With the simultaneous measurement of local particle density $n(\mathbf{r}, t)$, one has all the information needed to measure the integrands in Eq. (4.2). This spatial and temporal record of velocity divergence and particle concentrations is coupled together to obtain the area term of Eq. (4.2). The boundary term is obtained from particle concentrations at the periphery as they leave the field of view. This information when coupled with the velocity component perpendicular to the periphery, provides the boundary term. Figure. 4.3 shows both the area term (circles) and the boundary term (squares) of $S(t)$ in units of s^{-1}. These two curves are the primary results of this study.

It is seen from Fig. 4.3 that the dominant contribution comes from the area term, on which FF focus. After the system has reached a steady state (in roughly 0.2 s), both the area and boundary terms reach values of -1.82 $\pm$ 0.07 Hz and -0.60 $\pm$ 0.7 Hz respectively. It is apparent that the boundary term is hardly distinguishable from zero, though its uncertainty is appreciable.

The steady-state value of the area term, now to be called $\dot{S}_a(\infty)$, cannot be predicted from general considerations. However, if the system is highly chaotic, in the sense that it obeys SRB statistics [21, 19, 26]), $\dot{S}_a(\infty)$ should equal the sum of the two Lyapunov exponents charactering the motion of floaters:

$$\dot{S}_a(\infty) = -\int d\tau \langle \omega(t+\tau)\omega(t) \rangle = \lambda_1 + \lambda_2, \tag{4.4}$$

with the convention that $\lambda_1 > \lambda_2$.

These two Lyapunov exponents have not been measured in this experiment, but the ribbon-like clusters seen in Fig. 4.1 suggest one exponent is negative and the other positive. For SRB statistics, one expects smooth behavior of the particle density along the unstable direction (where $\lambda_1 > 0$) and a fractal distribution of $n(\mathbf{r})$ along the transverse direction corresponding to $\lambda_2 < 0$. These two exponents have been extracted from a computer simulation of clustering on the surface of a turbulent fluid, the starting point being the Navier-Stokes equation [9]. In that study, the experimental parameters were close to those of the present experiments. This study yields $\lambda_1 = +0.3$ Hz and $\lambda_2 =$ -2.0 Hz. The exponents have oppo-

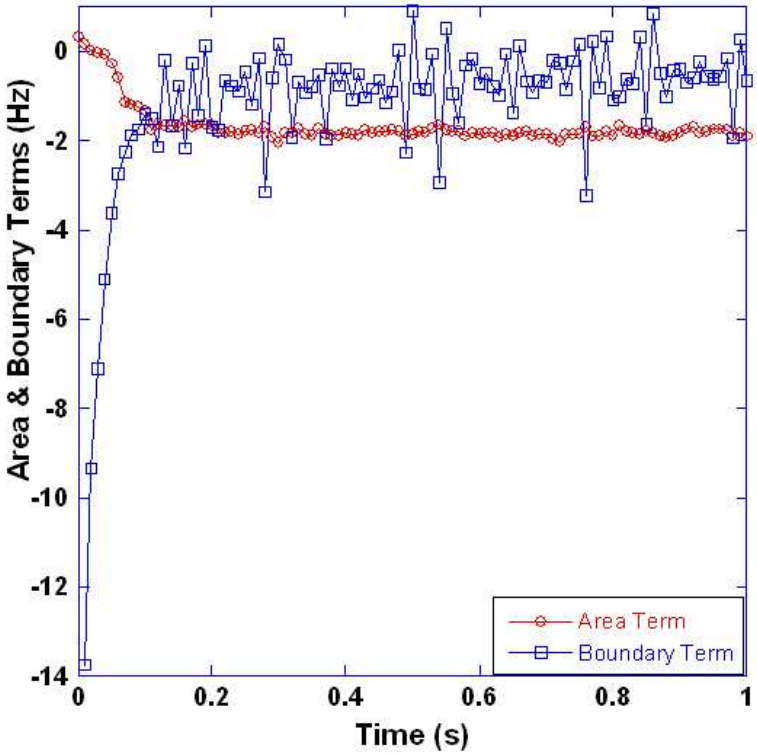

Figure 4.3: The production rate of entropy ($\dot{S}$) in Eq. 4.2. The Area Term (red circles) and Boundary Term (blue squares) in Eq. (4.2) reach steady state (0.2 s) within a fraction of the large eddy turnover time of turbulence (0.54 s).

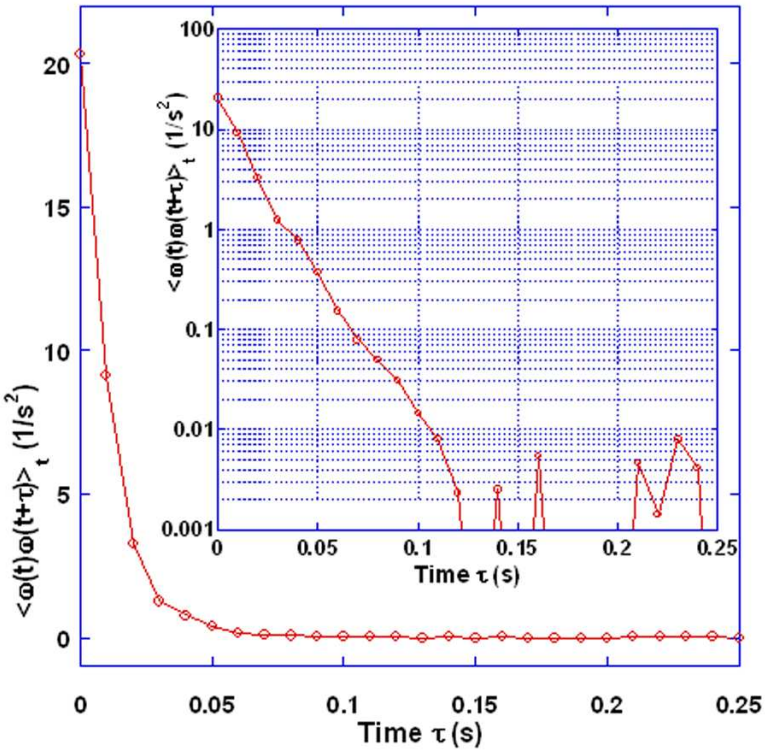

Figure 4.4: Temporal correlation $C_{div}(\tau)$ of the lagrangian velocity divergence $\omega(\mathbf{r},t) = \vec{\nabla}_2 \cdot \mathbf{v}(\mathbf{r},t)$ vs. time τ. It was calculated individually for velocity divergence time traces of 50000 lagrangian trajectories, and averaged to obtain the plot in the figure. The inset shows the same temporal correlation function in the log-linear scale. As is apparent, the decay is close to exponential with a decay constant of approximately 0.02 s. Beyond $\tau \simeq 0.1$ s, the signal has decayed into the noise.

site sign, as expected. Their sum, -1.7 Hz, agrees surprisingly well with the measured value, $\dot{S}_a(\infty)$ = -1.82 $\pm$ 0.07 Hz. In addition, $\dot{S}_a(\infty)$ is also expected to equal the time integral of the correlation function of lagrangian velocity divergence with a negative prefactor as seen in Eq. (4.4). The correlation function is shown in Fig. 4.4. It was extracted from an average of 50000 lagrangian trajectories. The area under this correlation function with a negative prefactor was calculated to be -0.3 Hz. This number is not at all in agreement with the above quoted values of $\dot{S}_a(\infty)$ and the sum of Lyapunov exponents. The primary assumption involved in the derivation of Eq. 4.4 is that the system is maximally chaotic, and therefore admits SRB statistics. This requirement is necessary in order for the entropy rate to equal the negative of the time integral of lagrangian velocity divergence correlation function as well as the sum of Lyapunov exponents. One expects therefore that either both expressions equal the entropy rate or neither. It is therefore perplexing that the sum of Lyapunov exponents come out in excellent agreement with measured entropy rate whereas the value obtained from the area under the lagrangian velocity divergence correlation function is off by an order of magnitude. The reason for this disagreement is not understood.

While the analysis of FF shows that the integral of the lagrangian divergence correlation is equal to the function $\dot{S}$, the theory, embodied in Eq. (4.3) makes no prediction about the form of $C_{div}(\tau) \equiv \langle \omega(\mathbf{r},t)\omega(\mathbf{r},t+\tau)\rangle$. Its time dependence is displayed in Fig. 4.4. As expected, the integral of $C_{div}(\tau)$ is finite. It is notable, however, that $C_{div}(\tau)$ decays almost exponentially, rather than as a power law. Its decay time is about 20 ms, which is approximately equal to the 15 ms-decay time of velocity gradients extracted from the same set of data.

4.4 CONCLUSION.

The statistical notions of temperature and entropy play a fundamental role in the theory of thermodynamics and equilibrium statistical mechanics. In the nonequilibrium steady state one is not yet sure of the appropriate definition of entropy (private communication with G. Gallavotti), and most attempts to define an effective or dynamical temperature have

thus far proved futile. An experiment was described where the turbulence is identified as a chaos generating mechanism and the time rate of entropy change for a system of floaters in compressible turbulence on a free surface is measured. The theoretical predictions made by FF are tested against the experimental measurements. It is surprising that out of two predictions arising from the assumption that the system admits SRB statistics, one clearly agrees with experimental measurements (sum of Lyapunov exponents) whereas the other fails and differs from measurements by more than an order of magnitude (negative time integral of lagrangian velocity divergence correlation function). Also measured for the first time is the lagrangian velocity divergence correlation function for the floaters which exhibits an exponential decay form with a decay constant of 20 ms, in accord with the characteristic time of velocity gradients measured in this experiment to be 15 ms.

5.0 TEST FOR THE FLUCTUATION RELATION IN COMPRESSIBLE TURBULENCE.

5.1 INTRODUCTION.

The classical Fluctuation Dissipation Theorem (FDT) [7, 39] relates the parameters that describe dissipation in a system in thermal equilibrium, e.g. its electrical or thermal conductivity, to the fluctuations that inevitably take place about the equilibrium state. In recent years there has been a strong effort to extend the FDT to systems that are very far from thermal equilibrium. The new theoretical results [32, 17, 30, 31, 19, 60] are often framed as a prediction concerning the ratio of two probabilities; that of a system's rate of entropy production to the rate of its entropy consumption. This new theorem will henceforth be called the Fluctuation Relation (FR). The FR concerns the probability density function of a variable related to the phase space contraction rate of an out-of-equilibrium system under study, this variable being a current **j** such as the flux of hear, momentum etc. The mean of **j** on a time interval τ is defined as:

$$J_\tau = \frac{1}{\tau}\int_t^{t+\tau} j(t')dt' \tag{5.1}$$

One is then interested in the probability distribution $\Pi(\Sigma_\tau)$ of the variable $\Sigma = J_\tau/J_\infty$, where $J_\infty = lim_{\tau\to\infty}J_\tau$ is the long time (stationary) average current for the system. If τ is larger than the characteristic time of the system, then the chaotic hypothesis [32] predicts that:

$$\frac{\Pi(+\Sigma_\tau)}{\Pi(-\Sigma_\tau)} = exp^{\tau\gamma\Sigma} \tag{5.2}$$

where γ is proportional to the phase space contraction rate. It is necessary to stress that the prediction holds for all values of Σ since the experimental results to be discussed below show marked deviations from the prediction beyond a certain value of Σ (in the appropriate notation which will be changed below).

The FR has been put to many experimental tests for transient [14, 74] as well as steady state measurements [16, 28, 15, 65], with both local and global quantities being measured for the steady state case. Often the measured quantity is some form of a flux that requires definition of a dynamical temperature in order to relate it to the entropy production rate. Working with few particles, Wang et. al. [74] and Carberry et. al. [14] have measured entropy rate fluctuations in their experiments. Described here is a turbulence experiment aimed at measuring fluctuations in the entropy rate $\dot{S}$ for a macroscopic system. The interpretation of the experiments does not require introduction of a dynamical temperature. The system being studied here is an assembly of a large number of tiny particles floating on the surface of a tank of water maintained in the turbulent steady state. The entropy S introduced here is that which appears in the the theory of dynamical systems [64]; it is not defined in terms of the heat input and the temperature. Rather, it is a measure of the rate of contraction of the system in the space of its dynamical variables. Its measurements are all in the lagrangian frame, so that it depends on time only rather than local space variables. That space is a two-dimensional one in which *floating* particles move on the surface of a turbulent tank of water. These particles form a compressible system, allowing the floaters to coagulate and permitting $dS(t)/dt = \dot{S}(t)$ to be nonzero. On the average, this quantity is negative, though it can take on both signs from one instant to another. The measurements can be compared with a prediction that $\dot{S}(t)$ is the sum of two Lyapunov exponents that describe motion in the plane (x, y) in which the floaters move.

Under the driving action of the turbulence beneath them, the floaters move erratically causing their local areal density $n(x, y, t)$ to fluctuate in space and time. The turbulence generates ripples on the surface but their amplitude is small and can be neglected [33]. The resulting motion of the floaters in this experiment is perhaps surprising. Even if the initial particle distribution on the surface is uniform, it does not remain so. Rather, the floaters flee fluid up-wellings and cluster into string-like structures around fluid down-wellings within a

fraction of a second as shown in Fig. 4.1, thus making the floaters a compressible system. The water on which they move is incompressible at all values of z including the surface ($z = 0$). Hence the two-dimensional divergence of the velocity at the surface must be non-zero, since $\vec{\nabla}_2 \cdot \vec{v} = \partial_x v_x + \partial_y v_y = -\partial_z v_z \neq 0$ (please refer to Chapter 3 for details of compressible turbulence at the surface).

5.2 THEORY.

The starting point of this work is an equation that relates $n(x, y, t)$ to a probability (see Chapter 3 and appendix A), thus allowing one to define an entropy for this system of floaters $S(t) = -\int d\mathbf{r}\ n(\mathbf{r}, t)\ \ln\ n(\mathbf{r}, t)$, where $d\mathbf{r} = dx\ dy$. Using this definition of entropy as well as particle conservation, Falkovich and Fouxon [25, 26] showed that the entropy production rate is:

$$\dot{S} = \int_A d\mathbf{r}\ n(\mathbf{r}, t)\omega(\mathbf{r}, t) + \int_{\partial A} n(\mathbf{r}, t) \ln\ n(\mathbf{r}, t)\mathbf{v}.d\mathbf{S}. \tag{5.3}$$

The first term on the right, the *area term*, represents the average entropy rate within the area of observation. The second term (*boundary term*) takes into account the fact that the floaters can leave the field of view A. The factor $\omega(\mathbf{r}, t) \equiv \vec{\nabla}_2 \cdot \vec{v}(\mathbf{r}, t)$ will be interpreted as the local entropy current or entropy rate. The area term in Eq. (5.3) is a weighted average of the local entropy current over A and hence is the global entropy production rate. In the previous experiment discussed in chapter 4 this global entropy rate was the quantity of interest. In that experiment the boundary term was measured to be relatively small and will not be discussed further. Note that if the particles were neutrally buoyant they would easily follow the fluid into the bulk and form an incompressible system. According to Eq. (5.3) $\dot{S} = 0$ in the incompressible bulk, in spite of the energy loss through viscous dissipation. Thus $\dot{S}$ is not a measure of heat loss.

In the experiments discussed here, individual particle trajectories are tracked in the lagrangian frame. For each particle trajectory, the velocity divergence ω, or local entropy

rate, is averaged over equal intervals of time τ. Typically τ lies in the range of hundreds of ms. The floaters stay in the camera's field of view for a time of the order of 1 s.

The Fluctuation Relation concerns the probability density of the random variable ω, or rather its value averaged over the the (adjustable) interval τ:

$$\sigma_\tau = \frac{-\frac{1}{\tau}\int_0^\tau \; dt \; \omega(\mathbf{r},t)}{\Omega}. \tag{5.4}$$

Here Ω is the long-time average of the entropy rate, a quantity that is negative, reflecting coagulation of the floaters:

$$\Omega = \lim_{\tau\to\infty} -\frac{1}{\tau}\int_0^\tau dt \; \omega(r,t).$$

Thus the value of Ω is independent of any lagrangian trajectory. The clustering of particles leads to a negative sign for the average entropy rate of the floating particles. The usual sign convention adopted for entropy rate in FR studies is positive. The sign convection adopted here is the conventional one and corresponds to a net positive average entropy rate for the floaters and their environment.

The ratio of the probability that σ_τ is positive to the probability that it is negative, is, according to the FR,

$$\ln \; [\frac{\Pi(+\sigma_\tau)}{\Pi(-\sigma_\tau)}] = \sigma_\tau \Omega \tau. \tag{5.5}$$

This equation is put to an experimental test under steady state conditions.

According to Eq. (5.5), it is more likely that σ_τ is positive than negative. The FR makes no prediction about the form of $\Pi(\sigma_\tau)$. Nevertheless, the present experiment yields this PDF for a rather wide range of σ_τ and for a span of averaging times τ (see Fig. 5.1). Note that σ_τ has been defined in such a way that its time-averaged value is unity.

The experimental scheme is identical to the one described in Chapter 4. In fact data set analysed here and in Chapter 3 is one and the same. Please refer to Chapter 3 for a detailed discussion of the experimental setup and the scheme by which data is collected.

Table 5.1: Statistical parameters for PDFs of Figure 5.1.

Statistics	$\tau = 5\tau_c$	$\tau = 10\tau_c$	$\tau = 15\tau_c$	$\tau = 20\tau_c$
Mean	1.03	0.96	1.01	0.87
Median	0.94	0.85	0.88	0.75
Std. Deviation	9.99	8.45	5.49	5.74
Skewness	-0.01	0.16	0.18	0.56
Kurtosis	12.84	16.18	10.00	12.98

5.3 ANALYSIS.

For the analysis discussed below, the experimentally obtained velocity fields are seeded with fictitious (surrogate) particles via computer programming. At $t = 0$, the 1024 x 1024 pixel grid of the velocity field is decorated with a uniform array of surrogate particles 6 pixels apart, providing $170^2 = 28900$ surrogate particles. Evolution of this initially uniform particle distribution is dictated by the experimental velocity fields. The particles are tracked by the program instant by instant in the lagrangian frame. Though some particles leave the field of view during the evolution time, they are tracked as long as they remain in it. For every surrogate particle that leaves A, a new particle is introduced at a random spatial point within it, thereby creating a new lagrangian trajectory. Real particles are substituted with surrogates in order to achieve particle tracking in the lagrangian frame.

The instantaneous velocity divergence field $\omega(\mathbf{r}, t)$ is calculated by taking component-wise spatial derivatives of the velocity field. As the surrogates evolve in time, driven by the underlying velocity fields, the velocity divergence along the lagrangian trajectory is obtained at every instant. Thus one has a time trace of the lagrangian velocity divergence for all evolving surrogates in the flow. Over 330,000 lagrangian trajectories were evolved in this experiment, of which velocity divergences were recorded for 80000 trajectories and employed in the FR analysis. The experiment runs over 20 s, corresponding to 37 large eddy turnover times ($\tau_0 = 0.54$ s), but most lagrangian trajectories have left the field of view within 3

turnover times.

5.4 RESULTS AND DISCUSSION.

The fluctuation relation is of interest when the system is in a transient state [22] as well as in the steady state. In this experiment, only steady-state measurements of σ_τ are reported. In practice, that means discarding the first 200 ms of the lagrangian velocity divergence time trace for each trajectory. This 200 ms interval was previously measured [4] to be the transient time period for the global entropy rate (area term of Eq. 5.3) to reach a steady state. The remaining time-trace of lagrangian velocity divergence was broken into windows of duration τ. The time-averaged value from each window represents the numerator of Eq. 5.4. Tracks that disappeared in less than (200 ms + τ) were discarded.

Figure 5.1 is a plot of $\ln[\Pi(\sigma_\tau)]$ *vs* σ_τ^2 for four values of τ in units of τ_c, the decay time of the velocity divergence correlation function, $C(\tau) = \langle\omega(\mathbf{r}, t+\tau)\omega(\mathbf{r}, t)\rangle$ [4]. Measurements made in the lagrangian frame established that this characteristic time is $\tau_c = 0.02$ s. If the PDFs were gaussian, these plots would be straight lines in this figure. The difference $\ln[\Pi(+\sigma_\tau)] - \ln[\Pi(-\sigma_\tau)] = \ln[\Pi(+\sigma_\tau)/\Pi(-\sigma_\tau)]$ is positive at all values of σ_τ in agreement with Eq. (5.5).

The parameters characterizing all four sets of PDF measurements are listed in Table 5.1. This table shows that the skewness of all the PDFs is quite small; the surface velocity divergence can take positive and negative values with almost equal likelihood. This was established in prior experiments where the PDF of $\vec{\nabla}_2 \cdot \vec{\mathbf{v}}$ was directly measured and simulated as well [18]. In that eulerian study the mean value of the divergence of the floaters was found to be almost zero. The non-gaussian form of the PDFs is also apparent in table 5.1, where one sees that the kurtosis is much greater than the gaussian value of 3.

Figure 4.3 shows the LHS of Eq. (5.5) (open circles) and the RHS of that equation (open squares) at the same values of τ/τ_c. The measurements in Fig. 5.5 are at odds with the FR (Eq. (5.5)) in two respects: First, they fall above the prediction at the smallest value of $\tau/\tau_c = 5$, lie below it in the opposite limit, $\tau/\tau_c = 20$ but support the FR at the intermediate

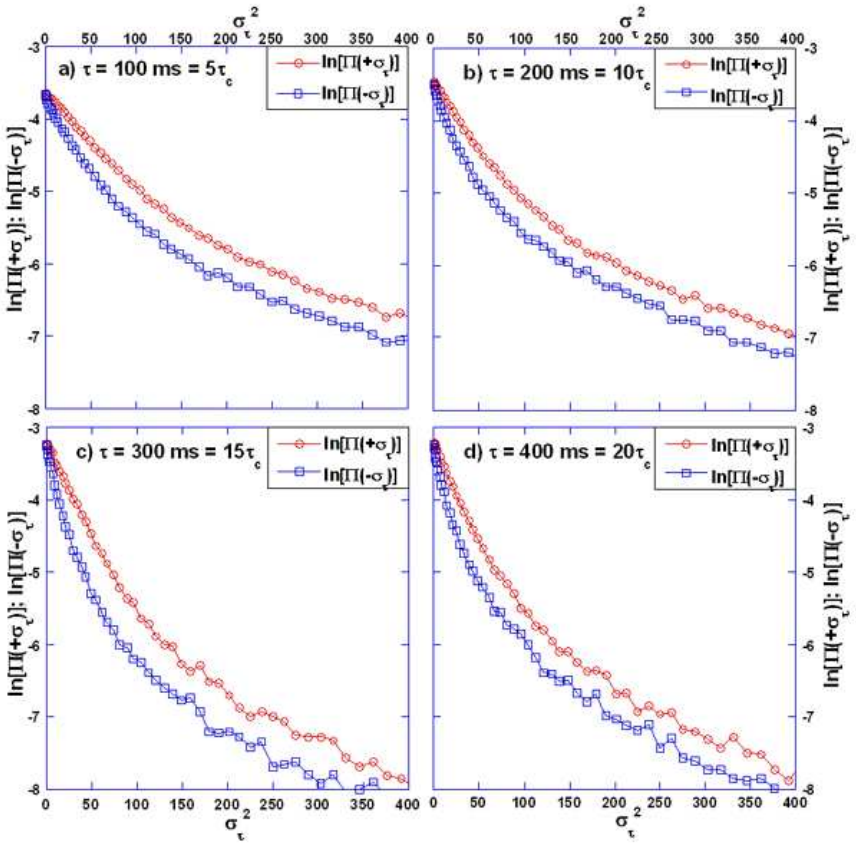

Figure 5.1: ln $[\Pi(\sigma_\tau)]$ *vs.* σ_τ^2 plotted for four values of τ in dimensionless units τ/τ_c ($\tau_c = 20$ ms) (a)$\tau/\tau_c = 5$, (b) $\tau/\tau_c = 10$, (c) $\tau/\tau_c = 15$, and (d) $\tau/\tau_c = 20$, for positive (open circles) and negative (open squares) values of the entropy current σ_τ. For a gaussian the decay is linear.

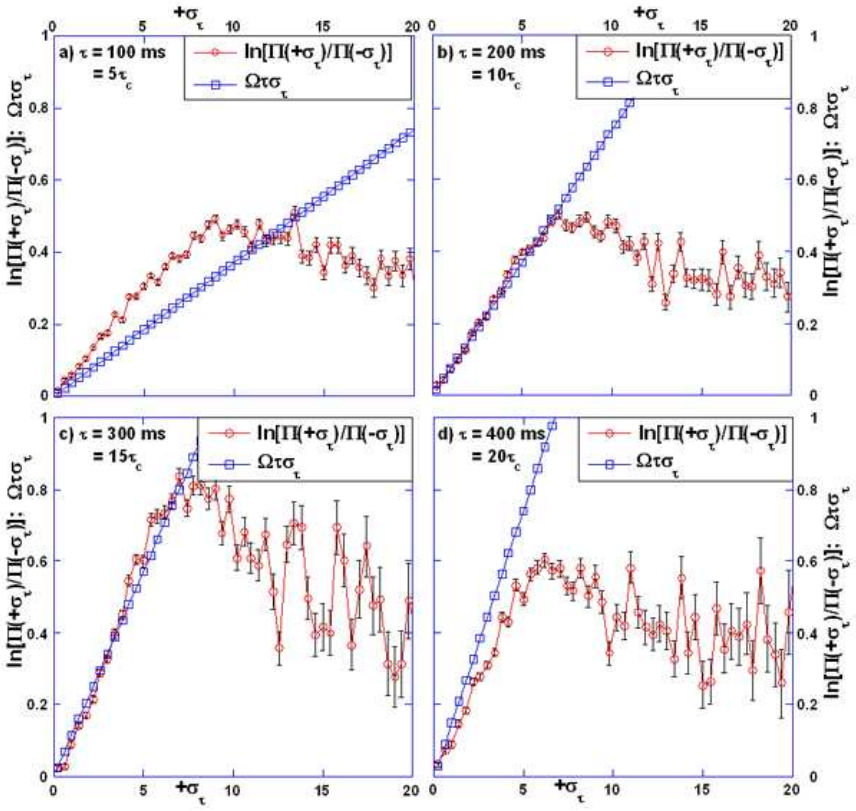

Figure 5.2: ln $[\Pi(+\sigma_\tau)/\Pi(-\sigma_\tau)]$ (open circles) plotted against σ_τ for the four dimensionless integration times (a) $\tau/\tau_c = 5$, (b) $\tau/\tau_c = 10$, (c) $\tau/\tau_c = 15$, and (d) $\tau/\tau_c = 20$. The solid line through the open squares is the RHS of Eq. (5.5).

values, $\tau/\tau_c = 10$ and 15. Second, when σ_τ exceeds 7 or so, the ratio $\mathcal{R} \equiv \ln\,[\frac{\Pi(+\sigma_\tau)}{\Pi(-\sigma_\tau)}]$ saturates and may even decrease measurably with increasing σ_τ. The convexity of $\mathcal{R}(\sigma_\tau)$ is expected under certain conditions [11]. It is however not clear if this explanation can account for the present observations. These measurements extend to larger values of σ_τ than other experiments and computer simulations [10]. Within the range $(0 \leq \sigma_\tau \leq 7)$, one sees that the statistical error is small. As σ_τ increases above 7, the number of data points N_B decreases, and the statistical noise is of the order of the measured $\sqrt{(N_B)}$. The error bars in Fig. (5.2) are $\pm\sqrt{(2 \times N_B)}$.

5.5 SUMMARY.

In summary, an experiment is reported where the local entropy rate σ_τ, a random variable, was measured in the lagrangian frame for a system consisting of an assembly of particles floating on a turbulent tank of water. The floaters form a compressible system, hence exhibits a nonzero value of the velocity divergence, which is equal to the entropy rate as defined in the work of Falkovich and Fouxon [25, 26]. The definition of σ_τ used here is not that of equilibrium thermodynamics but rather is closely related to that used in studies of chaotic systems [19, 64]. The calculations and measurements refer to the two-dimensional coordinate space in which the floaters move, not a four-dimensional phase space or the full phase space of the large number of floaters.

The experimental steady-state results agree with the fluctuation relation but only over a limited range of the averaging time τ. The PDFs themselves are notable in several respects: (1) they are only slightly skewed, (2) their mean values are small compared to their standard deviations from the mean, and (3) their shapes are different for positive and negative values of the dimensionless entropy rate σ_τ defined in Eq. (5.4). As the coagulation of the floaters implies, positive values the PDF are larger than the negative values at each entropy rate. While this is a study of the entropy rate in the steady state, the FR is also relevant for a system in the transient state [22]. Measurements of the transient type where the observations are qualitatively similar to those presented in Figs. 5.1 and 5.2 are not discussed here.

6.0 CONCLUSION.

6.1 SUMMARY

In summary, four experiments have been discussed that deal with various facets of the turbulence problem. They explore aspects of incompressible turbulence and compressible turbulence at a free surface within the hydrodynamic context with Kolmogorov's phenomenological theory of 1941 being the basis, as well as in the context of dynamical systems theory for which the turbulence is treated as a tool to generate chaos.

In Experiment 1, the finite size effects on downscale energy transfer rate and its backscatter frequency were studied both experimentally and numerically. In numerical simulations conducted by A. Pumir, the SPH approximation was applied which was found to be in good agreement with experimental results. The effectiveness of the SPH method was also established by re-analyzing experimental data by the SPH technique and cross-correlating its results with those obtained from Kolmogorov theory.

In Experiment 2, the eulerian third-order structure function ($S_3(r)$) and lagrangian second-order structure function ($D_2(\tau)$) were measured for compressible turbulence on a free surface for the first time. Despite violation of the incompressibility condition the measured $S_3(r)$ was shown to agree very well with the four-fifth law. The measured $D_2(\tau)$ was found to scale with a power-law exponent of $\tau^{1/2}$ as against the linear scaling in τ leading to a scaling mismatch between Eulerian and Lagrangian velocity statistics. No conclusive inferences or dimensional arguments were drawn from the lagrangian analysis of the data due to poor statistical convergence for higher order structure functions.

Experiment 3 involved a measurement of the steady state entropy production rate in compressible turbulence on a free surface. The recent theory of Falkovich and Fouxon was

tested against experimental measurements. The theoretical prediction requiring the entropy rate to equal the negative time integral of the lagrangian velocity divergence correlation function was found to be in disagreement with experimental results. However the measured entropy rate was equal to the sum of the system's Lyapunov exponents obtained from numerical simulations by Boffetta et. al.

Experiment 4 applied the local entropy rate fluctuations obtained from individual lagrangian tracer particles to test the steady state fluctuation theorem of Gallavotti and Cohen. The experimental results overshot theoretical predictions at early averaging times and undershot at late averaging times. The results were in very good agreement for intermediate averaging times over a range that exceeded prior experiments and numerical simulations.

Some of the experiments discussed here continue to be open problems. There are other ideas the author has thought about as a graduate student, but could not pursue for lack of equipment, time or other extraneous reasons. In the author's opinion these problems are worthy of experimental investigation either because they are important, or because they are interesting. These ideas are detailed in Appendix B for the benefit of those who probably share the author's opinion, and may choose to pursue them.

APPENDIX A

THEORY OF FALKOVICH AND FOUXON.

Consider a system driven out of thermal equilibrium into the nonequilibrium steady state. By the nonequilibrium steady state condition one implies that the rate of energy injection into the system equals its rate of dissipation of energy as heat. Falkovich and Fouxon consider such a nonequilibrium steady state process for an arbitrary physical system that can be described by the evolution of a density n which satisfies Liouville's continuity equation:

$$\frac{\partial n}{\partial t} + \vec{\nabla} \cdot (n\vec{v}) = 0 \tag{A.1}$$

Here the density $n(\mathbf{r}, t)$ could either be the density of points in phase space or of real particles in configuration space. Likewise $\vec{v}(\mathbf{r}, t)$ represents the velocity field that defines the phase space dynamics or evolution of particles in real space, depending upon the situation under consideration. The total mass is assumed to be conserved implying $\int n(\mathbf{r}, t) d\mathbf{r} = 1$. The Equilibrium condition for the system is characterized by a smooth measure for the density $n(\mathbf{r}, t)$, say of the microcanonical ensemble. This condition translates to a uniform or homogeneous distribution of points in phase/configuration space. Such distributions are subject to hydrodynamic evolution characterized by incompressible flow. In the Equilibrium condition, one therefore realizes the state of maximal Gibbs entropy.

$$S = -\int n(\mathbf{r})\ ln\ n(\mathbf{r}) d\mathbf{r} \tag{A.2}$$

specified by $n = 1/V =$ constant. Such a state is not stationary if the velocity field that drives

the evolution is compressible ($\omega = \vec{\nabla} \cdot \vec{v} \neq 0$). Under such compressible flow conditions, the density field $n(\mathbf{r}, t)$ becomes inhomogeneous and the Gibbs entropy decreases due to entropy flux from the system to the environment. This is usually interpreted as the contraction of phase space due to evolution of the strange attractor within the system's phase space towards which the phase points evolve as they follow the compressible hydrodynamical fields.

Consider a time-dependent formulation of Eq. A.2

$$S(t) = -\int d\mathbf{r} n(\mathbf{r}, t)\ ln\ n(\mathbf{r}, t) \tag{A.3}$$

Appling the continuity equation (Eq. A.1) to Eq. A.3 one can derive an exact expression for the system's entropy production rate.

$$\frac{\partial n}{\partial t} + \vec{\nabla} \cdot (n\vec{v}) = 0$$

$$\frac{\partial n}{\partial t} = -[n\omega + \vec{v} \cdot \vec{\nabla} n] \tag{A.4}$$

Consider $\vec{\nabla} \cdot (n\ ln\ n\ \vec{v})$:

$$\vec{\nabla} \cdot (n\ ln\ n\ \vec{v}) = n\ ln\ n\ \omega + n\vec{v} \cdot \vec{\nabla}\ ln\ n + \vec{v}\ ln\ n \cdot \vec{\nabla} n$$
$$\vec{\nabla} \cdot (n\ ln\ n\ \vec{v}) = n\ ln\ n\ \omega + \vec{v} \cdot \vec{\nabla} n + \vec{v}\ ln\ n \cdot \vec{\nabla} n$$

$$\vec{\nabla} \cdot (n\ ln\ n\ \vec{v}) = (1 + ln\ n)\vec{v} \cdot \vec{\nabla} n + n\ ln\ n\ \omega \tag{A.5}$$

Taking derivative of Eq. A.3 with respect to time t:

$$\dot{S} = -\int d\mathbf{r} \frac{\partial}{\partial t}[n(\mathbf{r}, t)\ ln\ n(\mathbf{r}, t)] \tag{A.6}$$

Consider the integrand in Eq. A.6:

$$\frac{\partial}{\partial t}[n(\mathbf{r}, t)\ ln\ n(\mathbf{r}, t)]$$
$$= ln\ n\ \frac{\partial n}{\partial t} + \frac{\partial n}{\partial t}$$

$$= (1 + ln\ n)\frac{\partial n}{\partial t}$$

Replacing $\frac{\partial n}{\partial t}$ with result from Eq. A.4:

$$\begin{aligned}
&\frac{\partial}{\partial t}[n(\mathbf{r},t)\ ln\ n(\mathbf{r},t)] \\
&= -(1 + ln\ n)(n\omega + \vec{v}\cdot\vec{\nabla}n) \\
&= -n\omega - n\ ln\ n\ \omega - (1 + ln\ n)\vec{v}\cdot\vec{\nabla}n
\end{aligned}$$

Plugging in the result of Eq. A.5 in above equation:

$$\frac{\partial}{\partial t}[n(\mathbf{r},t)\ ln\ n(\mathbf{r},t)] = -n\omega - \vec{\nabla}\cdot(n\ ln\ n\ \vec{v})$$

Plugging this back into Eq. A.6 one obtains:

$$\begin{aligned}
\dot{S} &= -\int_V d\mathbf{r}\frac{\partial}{\partial t}[n(\mathbf{r},t)\ ln\ n(\mathbf{r},t)] \\
&= \int_V d\mathbf{r}[n\omega + \vec{\nabla}\cdot(n\ ln\ n\ \vec{v})] \\
&= \int_V d\mathbf{r}n(\mathbf{r},t)\omega(\mathbf{r},t) + \int_V d\mathbf{r}\vec{\nabla}\cdot(n\ ln\ n\ \vec{v})
\end{aligned}$$

Converting second term in above equation to a surface integral, one obtains:

$$\dot{S} = \int_V d\mathbf{r}\ n(\mathbf{r},t)\omega(\mathbf{r},t) + \int_{\delta V} n\ ln\ n\ \vec{v}\cdot d\mathbf{S} \tag{A.7}$$

Eq. A.7 is the exact result quoted in Eq. 4.2, and forms the starting point for all analysis discussed in Chapter 4. For derivation of Eq. 4.4, the interested reader is referred to [25].

APPENDIX B

OPEN PROBLEMS AND SOME EXPERIMENTAL POSSIBILITIES.

B.1 EXPERIMENT 1: HIGHER ORDER LAGRANGIAN VELOCITY STATISTICS IN COMPRESSIBLE TURBULENCE AT A FREE SURFACE.

The results in chapter 3 were inconclusive partly due to insufficient statistics of lagrangian velocity differences. It is suggested that data be collected for a higher duration at lower frame rate of the high-speed camera, and the analysis be repeated. The author expects at least a tripling of the number of lagrangian trajectories for a 20 s time-record of the compressible flow. With the recent changes made to the tank, the author believes higher Re may be achievable for future datasets. Obtaining higher-order structure functions from such a dataset may allow one to elucidate an approximate dimensional form, although intermittency effects are expected to destroy such predictions for higher-order structure functions.

B.2 EXPERIMENT 2: TEST FOR INJECTION SCALE EFFECTS AT THE KOLMOGOROV SCALE.

Under Kolmogorov's 1941 theory (K41), one expects that no injection scale effects are observable in a fully developed inertial sub-range at high Re. It is conceivable therefore under K41 that one should not expect to see any injection scale fluctuations at the Kolmogorov

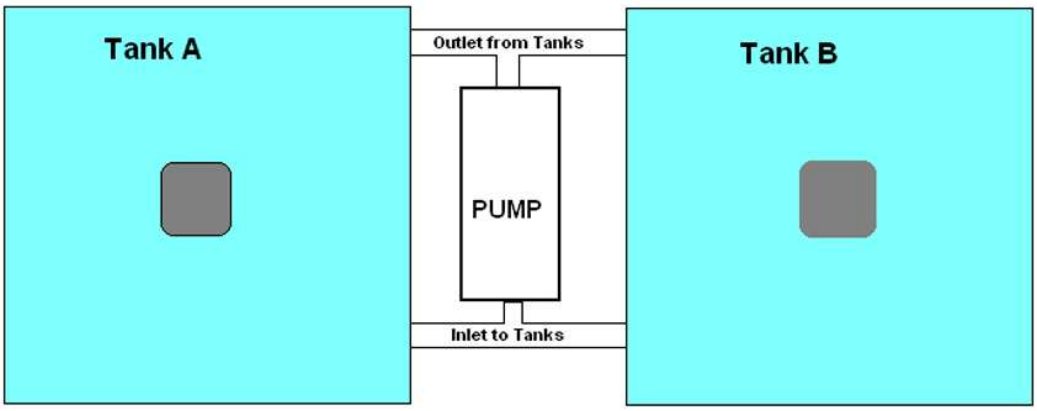

Figure B1: A hypothetical setup consisting of two tanks driven by a common injection source (pump). Two individual high-speed cameras are suspended above Tanks A and B, to simultaneously collect data from each tank independently.

scale η. However the author has found no experimental evidence to this effect. In fact the recent theory of zero modes [27] and statistically preserved structures would expect a "leak" or direct energy transfer from the injection scale to the dissipative scale. An experimental confirmation would be a significant result in the author's opinion. A scheme to test this possibility is suggested here.

Consider a hypothetical experimental setup involving two tanks driven by a common pump. Hence both tanks A and B share a common injection source. A schematic block diagram of two tanks with two individual high-speed cameras suspended overhead is sketched in fig. B1. It is natural therefore that any injection scale fluctuations should be simultaneously felt in turbulence generated in both tanks. The procedure to conduct an experiment in this setup is detailed below.

1) Synchronize both high-speed cameras to start data collection at the same time. Drive the pump to generate turbulence simultaneously in both tanks and collect data once the turbulence reaches a steady state. The data should be collected through a cut in the incompressible bulk since this experiment pertains to incompressible turbulence governed by K41.

2) Process raw datasets from Tank A and B through the particle tracking program and obtain the corresponding velocity field snapshots.

3) Compute the rate of energy dissipation for ε_d at each instant, and obtain individual time-traces $\varepsilon_d^A(t)$ and $\varepsilon_d^B(t)$ and subtract the average value out, so one has the pure fluctuations.

4) Calculate the normalized cross-correlation of the two time traces:

$$X_d(\tau) = \frac{\langle \varepsilon_d^A(t)\varepsilon_d^B(t+\tau)\rangle}{\sqrt{\langle(\varepsilon_d^A)^2\rangle}\sqrt{\langle(\varepsilon_d^B)^2\rangle}} \tag{B.1}$$

5)Ideally, if the expectation of K41 holds true then $X_d(\tau) = 0$ identically for all τ. If instead $X_d(\tau) \neq 0$ but has some small positive value, it would imply the dissipative scale fluctuations in both tanks are correlated. Since the only aspect common to Tanks A and B is the injection source, the source of correlation can only arise at the injection scale. This would be convincing proof of existence of injection scale fluctuations at the dissipative scale.

The requirement of high Re is crucial to this experiment, so that the expectation of a fully developed inertial range is achieved in the first place. A variant of this experiment can be performed in the existing tank by dividing the tank in two by fixing a plank. Although this experiment can be done with a single camera placed exactly above the plank, in order to negate any boundary wall effects arising from the plank, it is advised that two cameras be employed to record data in each half of the tank.

B.3 EXPERIMENT 3: PRIMITIVE TEST FOR FINITE TRANSIT TIME OF ENERGY THROUGH INERTIAL SUBRANGE.

Consider a setup comprising a tank of water maintained in a turbulent steady state by a pump controlled by a sinusoidally driven torque drive. It is possible to control the sinusoidal modulation of the torque drive using a signal generator. Modulate the torque drive at a frequecy of inverse large eddy turnover time of turbulence and collect turbulent velocity data from a cut through the incompressible bulk flow of the tank. Compute a time-trace of the energy dissipation rate $\varepsilon_d(t)$ from the velocity fields, and calculate the normalized

cross-correlation of the sine wave with the energy dissipation rate. Assume the mean has been subtracted out of both signals.

$$X(\tau) = \frac{\langle sin(\omega t)\varepsilon_d(t+\tau)\rangle}{\sqrt{0.5}\sqrt{\langle \varepsilon_d^2 \rangle}} \tag{B.2}$$

If a phase shift ϕ is observed in $X(\tau)$, and the phase-shifted peak of the cross-correlation curve occurs at a time τ comparable to the large-eddy turnover time of turbulence, one has preliminary proof of finite transfer time for energy to transit from injection scale to the dissipative scale. This scheme is a variant of the mean-field theoretic idea of modulated turbulence proposed by A. von der Heydt et. al. [73]. The sinusoidal modulation acts as a lock-in mechanism in this proposed experiment.

B.4 EXPERIMENT 4: 2D MODULATED TURBULENCE WITH ACTIVE GRID.

The author had attempted to study modulated turbulence in quasi-2D turbulent fluids using soap films on a scheme suggested by A. von der Heydt et. al. [73]. The turbulence was modulated by a solenoid valve that controlled flow of soap solution by opening and closing periodically. A serious problem with this scheme was that the valve could not be driven at high frequencies where all the interesting effects were predicted. It is possible to generate modulated turbulence by fixing an audio speaker to a grid with saw teeth (comb) that generates the turbulence in the soap film. Modulation of the speaker with an acoustic oscillator can drive the comb sinusoidally in and out of the film, thereby modulating the outer-scale l_0 of turbulence. This in turn should achieve the modulation of turbulent flow at higher frequencies.

APPENDIX C

KOLMOGOROV THEORY OF 1941 (K41)

All analysis discussed in Chapters 2 and 3 relies on the Kolmogorov theory of 1941 (K41). A short discussion of the main aspects of K41 is provided here. There are two main theoretical predictions that appear in K41. The first is the celebrated four-fifth law which is exact, and the second is a dimensional prediction arising from the four-fifth law that the n^{th} order structure function of longitudinal velocity differences $S_n(r) \equiv \langle(\Delta u_L(r))^n\rangle \sim (\bar{\varepsilon}r)^{n/3}$. These predictions are based on three hypotheses:

Hypothesis 1 (H1): In the limit of infinite Reynolds numbers, all the possible symmetries of the Navier-Stokes Equation (Eq. 1.1), usually broken by the mechanisms producing turbulent flow, are restored in a statistical sense at small scales away from the boundaries.

The small scales are spatial scales r smaller than the integral scale l_0 of turbulence. This hypothesis is interpreted as small scale homogeneity of velocity increments.

$$\Delta u(x,r) \equiv u(x+r) - u(x) \tag{C.1}$$

Specifically it is assumed that:

$$\Delta u(x+\rho,r) = \Delta u(x,r) \tag{C.2}$$

for all increments r and all spatial displacements ρ which are small compared to integral scale l_0.

Hypothesis 2 (H2): Under the same assumptions as in H1, the turbulent flow is self-similar at small scales.

This implies there exists a unique scaling exponent h such that:

$$\Delta u(x, \lambda r) = \lambda^h \Delta u(x, r) \tag{C.3}$$

for all x and all increments r and λl small compared to integral scale l_0. As will be seen later, this unique scaling exponent is predicted to be 1/3 under K41 and is determined via the four-fifth law. This hypothesis was referred to by Kolmogorov as the second hypothesis of similarity, and is today referred to as Kolmogorov's second self-similarity hypothesis.

Hypothesis 3 (H3): Under the same assumptions as in H1, the turbulent flow has a non-vanishing mean rate of dissipation ε per unit mass.

C.1 THE FOUR-FIFTH LAW.

Four-fifth law: *In the limit of infinite Reynolds number, the third order (longitudinal) structure function of homogeneous isotropic incompressible turbulence evaluated for increments r small compared to the integral scale l_0, is given in terms of the mean rate of energy dissipation per unit mass $\overline{\varepsilon}$ (assumed to remain finite and non-vanishing) by:*

$$\langle \Delta u_L(r))^3 \rangle = -\frac{4}{5}\overline{\varepsilon} r \tag{C.4}$$

This law is derivable directly from the Navier-Stokes Equation (Eq. 1.1) under the assumptions of homogeneity, isotropy, incompressibility and hypothesis H3 above. It is one of the most important results ever dervied in fully developed turbulence because it is both exact and non-trivial.

Note: Since it is understood that one is looking at the longitudinal component of velocity differences, the subscript L shall henceforth be dropped. Since it is also understood that one is interested in the mean rate of energy dissipation, the overline over ε will be dropped.

At this point it is worth mentioning that Kolmogorov's derivation itself relied on another relation derived earlier by Theodore von Kármán and Howarth [72] and later generalized to anisotropic flows by Monin, known as the Kárman-Howarth-Monin relation.

C.1.1 THE KÁRMÁN-HOWARTH-MONIN RELATION.

Homogeneous (but not necessarily isotropic) solutions of the Navier-Stokes equation Eq. 1.1 satisfy:

$$\begin{aligned}\varepsilon(r) &= -\frac{1}{4}\nabla_r \cdot \langle |\Delta u(r)|^2 \Delta u(r)\rangle \\ &= -\partial_t \tfrac{1}{2}\langle u(x)\cdot u(x+r)\rangle + \langle u(x)\cdot \tfrac{f(x+r)+f(x-r)}{2}\rangle \\ &\qquad +\nu\nabla_r^2\langle u(x)\cdot u(x+r)\rangle\end{aligned}$$

where ∇_r denotes partial derivatives with respect to the spatial increment r, the angular brackets denote a spatial average on x, and $f(x,t)$ is the forcing term.

This relation leads to an important interpretation. If we hold the viscosity $\nu > 0$ fixed and let the sepration $r \to 0$ in the above equation, the term $\nabla_r \cdot \langle |\Delta u(r)|^2 \Delta u(r)\rangle$ tends to zero. Inded, velocity increments vary linearly for very small increments (assuming smoothness for $\nu > 0$). One is then left with the relation:

$$\partial_t \frac{1}{2}\langle u^2\rangle = \langle f(x)\cdot u(x)\rangle + \nu\langle v(x)\cdot\nabla^2 u(x)\rangle \tag{C.5}$$

an equation which expresses that the only changes in the mean energy come from the input through the force and the viscous energy dissipation. Kolmogorov's important result extended this to the case when $r \neq 0$, which led to the energy-flux relation, we know now as the four-fifth law.

C.1.2 KOLMOGOROV'S EXTENSION TO THE KÁRMÁN-HOWARTH-MONIN RELATION.

It is easier to work the remaining steps in fourier space where the energy balance can be easily expressed scale-by-scale in wavenumber space. The scale-dependent energy budget can be arrived at directly from the Navier-Stokes equation (Eq. 1.1), which in k-space reads:

$$\partial_t \mathcal{E}_K + \Pi_K = \mathcal{F}_K - 2\nu\Omega_K \tag{C.6}$$

where $\mathcal{E}_K$ is the cumulative energy for all wavenumbers $k \leq K$, Π_K is the energy flux, $\mathcal{F}_K$, and Ω_K is the enstropy. The cumulative energy flux Π_K across all scales $k \leq K$ (see [29] page 80) can be recast as:

$$\Pi_K = \frac{1}{2\pi^2} \int d^3r \ \frac{sin(Kr)}{r} \nabla_r \cdot [\varepsilon(r) \frac{\mathbf{r}}{r^2}] \tag{C.7}$$

Substituting $\varepsilon(r)$ with the Kármán-Howarth-Monin relation gives:

$$\Pi_K = -\frac{1}{8\pi^2} \int d^3r \ \frac{sin(Kr)}{r} \nabla_r \cdot [\frac{\mathbf{r}}{r^2} \nabla_r \cdot \langle |\Delta u(r)|^2 \Delta u(r) \rangle] \tag{C.8}$$

This energy flux relation is enough to derive the value of scaling exponent h = 1/3 within the K41 framework. However introducing the additional assumption of isotropy at this point allows one to recast the above result in terms of the experimentally measurable third-order Eulerian structure function $S_3(r) \equiv \langle (\Delta u(r))3 \rangle$ (see [29] page 81 for proof):

$$\Pi_K = -\frac{1}{6\pi} \int_0^\infty dr \frac{sin(Kr)}{r} (1 + r\partial_r)(3 + r\partial_r)(5 + r\partial_r) \frac{S_3(r)}{r} \tag{C.9}$$

At this point, in addition to assumptions of homogeneity and isotropy of the incompressible turbulent flow, we introduce three assumptions specific to fully developed turbulence:

(1) The driving force $f(x,t)$ acts only at large scales. Specifically it is assumed tht the force makes no direct contribution to spatial scales below the integral scale or $K_C = 1/l_0$ in k-space.

(2) For large times, the solution of the Navier-Stokes equation approaches a statistically stationary value with a finite mean energy per unit mass.

(3) In the limit of infinite Reynolds number ($\nu \to 0$), the mean energy dissipation per unit mass $\varepsilon(\nu)$ tends to a finite positive limit (this is hypothesis H3).

Let us consider the consequences of these assumptions. Stationarity implies that the time-derivative terms in Eq. C.9 can be omitted, giving $\Pi_K = \mathcal{F}_K - 2\Omega_K$.

Consider the forcing term $\mathcal{F}_K$, for $K \gg K_C$. Using assumption 1 above, one has $\mathcal{F}_K = \langle f_K^< \cdot u \rangle \simeq \langle f \cdot u \rangle = \varepsilon(\nu)$.

Consider the dissipation term, in the limit of viscosity approaching zero, we see $lim_{\nu \to 0} 2\nu\Omega_K = 0$.

From the above properties, one immediately sees that the flux term $lim_{\nu \to 0}\Pi_K = \varepsilon$ for all wavenumbers $k \gg K_C$. This implies, that in the statistically stationary state, the energy flux is independent of the scale under consideration and equal to the energy input/dissipation, provided that there is no direct energy injection ($K \gg K_C$) and no direct dissipation ($\nu \to 0$). Combining this relation with Eq. C.9 for the energy flux, we have:

$$\Pi_K = -\int_0^\infty dz \; \frac{sin\ z}{z} F(z/K) = \varepsilon \tag{C.10}$$

where $z = Kr$ and $F(r) = (1 + r\partial_r)(3 + r\partial_r)(5 + r\partial_r)\frac{S_3(r)}{6\pi r}$.

Observe that the large K behavior of the integral above involves only the small-r behavior of F(r), using the identity $\int_0^\infty dz \; (sinz/z) = \pi/2$, one has $F(r) \simeq -\frac{2}{\pi}\varepsilon$.

Substituting it in Eq. C.10, one has a third order differential equation for $S_3(r)$ whose only solution that approaches zero as $r \to 0$ is $S_3(r) = -\frac{4}{5}\varepsilon r$.

C.2 KOLMOGOROV-OBUKHOV LAW AND THE SELF-SIMILARITY HYPOTHESIS.

The four-fifth law leads to another prediction for n^{th} order structure functions for $n \neq 3$. As is now known the four-fifth law states $\langle (\Delta u_L(r))^3 \rangle = -\frac{4}{5}\bar{\varepsilon} r$, where $\Delta u_L(r)$ is the longitudinal velocity increment (or longitudinal component of velocity differences separated by a spatial scale r). With hypothesis H2 above, under rescaling of the spatial increment r by a factor λ, the LHS of four-fifth law changes by a factor λ^{3h}, while the RHS changes by a factor λ.

We now examine the consequences of structure functions of longitudinal velocity differences at inertial-range separations, assuming homogeneity and isotropy. We also assume structure functions of positive order $n > 0$ are finite, and define the n^{th} order structure function as $S_n(r) = \langle(\Delta u_L(r))^n\rangle$. From the self-similarity hypothesis H2, one can directly infer using dimensional arguments that $S_n(r) \propto r^{n/3}$. Since $(\overline{\varepsilon}r)^{n/3}$ has exactly the same dimensions as $S_n(r)$, one then has $S_n(r) = C_p\overline{\varepsilon}^{n/3}r^{n/3}$.

This leads to the prediction for the second-order structure function which gives, $S_2(r) \sim (\overline{\varepsilon}r)^{n/3}$. The second-order structure function has units of energy, and when fourier transformed into k-space, gives the energy spectrum $E(k) \sim k^{-5/3}$. This prediction works well for low order structure functions, and fails for $n > 3$, a problem now known as the anomalous-scaling or multi-scaling problem.

BIBLIOGRAPHY

[1] L. Angheluta, R. Benzi, L. Biferale, I. Procaccia, and F. Toschi. On the anomalous scaling exponents in nonlinear models of turbulence. *Preprint*, nlin.CD/0602002, 2006.

[2] F. Anselmet, Y. Gagne, E. J. Hopfinger, and R. A. Antonia. High-order velocity structure functions in turbulent shear flow. *J. Fluid. Mech.*, 140:63, 1984.

[3] F. Argoul, A. Arnéodo, G. Grasseau, Y. Gagne, E. J. Hopfinger, and U. Frisch. Wavelet analysis of turbulence reveals the multifractal nature of the richardson cascade. *Nature*, 338:51, 1989.

[4] M. M. Bandi, W. I. Goldburg, and J. R. Cressman. Measurement of entropy production rate in compressible turbulence. To be published.

[5] M. M. Bandi, W. I. Goldburg, J. R. Cressman, and A. Pumir. Energy flux fluctuations in a finite volume of turbulent flow. *Phys. Rev. E*, 73:026308, 2006.

[6] G. K. Batchelor. *The Theory of Homogeneous Turbulence.* Cambridge University Press, Cambridge, 1948.

[7] H. B.Callen and T. A. Welton. Irreversibility and generalized noise. *Phys. Rev.*, 83:34, 1951.

[8] R. Benzi, G. Paladin, G. Parisi, and A. Vulpiani. On the multifractal nature of fully developed turbulence and chaotic systems. *J. Phys.*, A17:3521, 1984.

[9] G. Boffetta, J. Davoudi, B. Eckhardt, and J. Schumacher. Lagrangian tracers on a surface flow: The role of time correlations. *Phys. Rev. Lett*, 93:134501, 2004.

[10] F. Bonetto, G. Gallavotti, and P. L. Garrido. Chaotic principle: An experimental test. *Physica D*, 105:226, 1997.

[11] F Bonetto, G. Gallavotti, A. Guiuliani, and F. Zamponi. *Math-ph/0601683.*, 2006.

[12] S. T. Bramwell, P. C. W. Holdsworth, and J.-F. Pinton. Universality of fluctuations in turbulence and critical phenomena. *Nature*, 396:552, 1998.

[13] O. Cadot and J.-H. Titon. On the relationship of the injected power between constant torque forcing and constant velocity forcing of fully turbulent flows. *Phys. Fluids*, 16:2140, 2004.

[14] D. M. Carberry, J. C. Reid, G. M. Wang, D. J. Searles, and D. J. Evans. Fluctuations and irreversibility: An experimental demonstration of a second-law-like theorem using a colloidal particle held in an optical trap. *Phys. Rev. Lett.*, 92:140601, 2004.

[15] S. Ciliberto, N. Garnier, J.-F. Pinton, and R. Ruiz-Chavarria. Experimental test of the gallavotti-cohen fluctuation theorem in turbulent flows. *Physica A*, 340:240, 2004.

[16] S. Ciliberto and C. Laroche. An experimental test of the gallavotti-cohen fluctuation theorem. *J. Phy. IV (France)*, 8:215, 1998.

[17] E. G. D. Cohen. Dynamical ensembles in statistical mechanics. *Physica A*, 240:43, 1997.

[18] J. R. Cressman, J. Davoudi, W. I. Goldburg, and J. Schumacher. Eulerian and lagrangian studies in surface flow turbulence. *New Journal of Physics*, 6:53, 2004.

[19] J. R. Dorfman. *An Introduction to Chaos in Nonequilibrium Statistical Mechanics.* Cambridge University Press, Cambridge, 1999.

[20] J. Duchon and R. Robert. Inertial energy dissipation for weak solutions of incompressible euler and navier-stokes equations. *Nonlinearity*, 13:249, 2000.

[21] J.-P. Eckmann and D. Ruelle. Ergodic theory of chaos and strange attractors. *Rev. Mod. Phys.*, 57:617, 1985.

[22] D. J. Evans and Debra J. Searles. Equilibrium microstates which generate second law violating steady states. *Phys. Rev. E.*, 50:1645, 1994.

[23] G. L. Eyink. Local 4/5-law and energy dissipation anomaly in turbulence. *Nonlinearity*, 16:137, 2003.

[24] G. L. Eyink and K. R. Sreenivasan. Onsager and the theory of hydrodynamic turbulence. *Rev. Mod. Phys.*, 78:87, 2006.

[25] G. Falkovich and A. Fouxon. Entropy production away from the equilibrium. *Preprint nlin.CD/0312033*, 2003.

[26] G. Falkovich and A. Fouxon. Entropy production and extraction in dynamical systems and turbulence. *New Journal of Physics*, 6:11, 2004.

[27] G. Falkovich, K. Gawedzki, and M. Vergassola. Particles and fields in fluid turbulence. *Rev. Mod. Phys.*, 73:913, 2001.

[28] K. Feitosa and N. Menon. Fluidized granular medium as an instance of the fluctuation theorem. *Phys. Rev. Lett.*, 92:164301, 2004.

[29] U. Frisch. *Turbulence: The legacy of A. N. Kolmogorov*. Cambridge University Press, Cambridge 1995.

[30] G. Gallavotti. Chaotic dynamics, fluctuations, nonequilibrium ensembles. *Chaos*, 8:384, 1998.

[31] G. Gallavotti. Entropy production and thermodynamics of nonequilibrium stationary states. *Chaos*, 14:680, 2004.

[32] G. Gallavotti and E. G. D. Cohen. Dynamical ensembles in nonequilibrium statistical mechanics. *Phys. Rev. Lett.*, 74:2694, 1995.

[33] W. I. Goldburg, J. R. Cressman, Z Vörös, B. Eckhardt, and J. Schmacher. Turbulence in a free surface. *Phys. Rev. E*, 63:065303(R), 2001.

[34] J. P. Gollub and H. L. Swinney. Onset of turbulence in a rotating fluid. *Phys. Rev. Lett.*, 35:927, 1975.

[35] S. N. Gurbatov, S. I. Simdyankin, E. Aurell, U. Frisch, and G. Tóth. On the decay of burgers turbulence. *J. Fluid Mech.*, 344:339, 1997.

[36] W. Heisenberg. Zur statistischen theorie der turbulenz. *Zeit. f. Phys.*, 124:628, 1948.

[37] B. Hof, C. W. H. van Doorne, J. Westerweel, F. T. M. Nieuwstadt, H. Faisst, B. Eckhardt, H. Wedin, R. R. Kerswell, and F. Waleffe. Experimental observation of nonlinear traveling waves in turbulent pipe flow. *Science*, 305:1594, 2004.

[38] A. N. Kolmogorov. Dissipation of energy in the locally isotropic turbulence. *Doklady Akad. Nauk SSSR*, 32:16, 1941.

[39] R. Kubo. The fluctuation-dissipation theorem. *Rep. Prog. Phys.*, 29:255, 1966.

[40] L. D. Landau and E. M. Lifschitz. *Fluid Mechanics.* Pergamon Press, Oxford, 1959.

[41] J. L. Lebowitz. Boltzmann's entropy and time's arrow. *Physics Today*, 46:9:32, 1993.

[42] Y. Li and C. M. Meneveau. Origin of non-gaussian statistics in hydrodynamic turbulence. *Phys. Rev. Lett.*, 95:164502, 2005.

[43] A. Liberazon, B. Lüthi, M. Guala, W. Kinzelbach, and A. Tsinober. Experimental study of the structure of flow regions with negative turbulent kinetic energy production in confined three-dimensional shear flows with and without buoyancy. *Phys. Fluids*, 17:095110, 2005.

[44] J. B. McLaughlin and P. C. Martin. Transition to turbulence of a statistically stressed fluid. *Phys. Rev. Lett.*, 33:1189, 1974.

[45] C. M. Meneveau and K. R. Sreenivasan. The multifractal spectrum of the dissipation field in turbulent flows. *Nucl. Phys. B. Proc. Suppl.*, 2:49, 1987.

[46] J. J. Monaghan. Smooth particle hydrodynamics. *Ann. Rev. Astron. Astrophys.*, 30:543, 1992.

[47] A. S. Monin and A. M. Yaglom. Statistical fluid mechanics. *Statistical Fluid Mechanics*, Vol. 2, MIT Press, Boston, 1975.

[48] N. Mordant, J. Delour, E. Léveque, A. Arnéodo, and J.-F. Pinton. Long time correlations in lagrangian dynamics: A key to intermittency in turbulence. *Phys. Rev. Lett.*, 89:254502, 2002.

[49] N. Mordant, P. Metz, O. Michel, and J.-F. Pinton. Measurement of lagrangian velocity in fully developed turbulence. *Phys. Rev. Lett.*, 87:214501, 2001.

[50] L. Mydlarski and Z. Warhaft. On the onset of high-reynolds-number grid-generated wind tunnel turbulence. *J. Fluid Mech.*, 320:331, 1996.

[51] Q. Nie and S. Tanveer. A note on third-order structure functions in turbulence. *Proc. R. Soc. Lond. A.*, 455:1615, 1999.

[52] J. Nikuradse. Strömungsgesetze in rauhen rohren. *vDI Forschungsheft (1933), [in English, in Technical Memorandum 1292, National Advisory Committee for Aeronautics (1950)]*, 361, 1933.

[53] G. Parisi and U. Frisch. On the singularity structure of fully developed turbulence. *Turbulence and Predictability in Geophysical Fluid Dynamics, Proceed. Intern. School of Physics 'E. Fermi',eds M. Ghil, R. Benzi and G. Parisi. North-Holland, Amsterdam, 1983*, page 84, 1985.

[54] J.-F. Pinton and P. C. W. Holdsworth. Power fluctuations in a closed turbulent shear flow. *Phys. Rev. E*, 60:R2452, 1999.

[55] A. Pumir and B. Shraiman. Lagrangian particle approach to large eddy simulations of hydrodynamic turbulence. *J. Stat. Phys.*, 113:693, 2003.

[56] A. Pumir, B. Shraiman, and M. Chertkov. The lagrangian view of energy transfer in turbulent flow. *Europhys. Lett.*, 56:379, 2001.

[57] O. Reynolds. An experimental investigation of the circumstances which determine whether the motion of water shall be direct or sinuous, and of the law of resistance in parallel channels. *Phil. Trans. Roy. Soc. Lond.*, 174:935, 1883.

[58] L. F. Richardson. *Weather Prediction by Numerical Process.* Cambridge University Press, Cambridge, 1922.

[59] Michael K. Rivera. The inverse energy cascade of two-dimensional turbulence. *PhD. Thesis, University of Pittsburgh*, 2000.

[60] D. Ruelle. Smooth dynamics and new theoretical ideas in nonequilibrium statistical mechanics. *J. Stat. Phys.*, 95:393, 1999.

[61] D. Ruelle. *Chance and Chaos.* Princeton University Press, Princeton, New Jersey, 1991.

[62] D. Ruelle and L. A. R. di Brozolo. *Chaotic Evolution and Strange Attractors.* Cambridge University Press, Cambridge, 1989.

[63] D. Ruelle and F. Takens. On the nature of turbulence. *Comm. Math. Phys.*, 20:167, 1971.

[64] H. G. Schuster and W. Just. *Deterministic Chaos: An Introduction.* John Wiley & Sons, 4th Edition, 2005.

[65] X.-D. Shang, P. Tong, and K.-Q. Xia. Test of steady-state fluctuation theorem in turbulent rayleigh-bénard convection. *Phys. Rev. E*, 72:015301(R), 2005.

[66] K. R. Sreenivasan, B. Dhruva, and I. S. Gil. The effects of large scales on the inertial range in high-reynolds-number turbulence. chao-dyn/9906041, 1999.

[67] P. Tabeling, G. Zocchi, B. Belin, J. Maurer, and H. Willaime. Probability density functions, skewness, and flatness in large reynolds number turbulence. *Phys. Rev. E*, 53:1613, 1996.

[68] B. Tao, J. Katz, and C. Meneveau. Statistical geometry of subgrid-scale stresses determined from holographic particle image velocimetry measurements. *J. Fluid. Mech.*, 457:35, 2002.

[69] G. I. Taylor. Eddy motion in the atmosphere. *Phil. Trans. R. Soc. A.*, 215:1, 1915.

[70] G. I. Taylor. Statistical theory of turbulence. *Proc. R. Soc. Lond. A*, 151:421, 1935.

[71] M. A. Taylor, S. Kurien, and G. L. Eyink. Recovering isotropic statistics in turbulence simulations: The kolmogorov 4/5th law. *Phys. Rev. E.*, 68:026310, 2003.

[72] Kármán T. von and Howarth L. On the statistical theory of isotropic turbulence. *Proc. R. Soc. Lond. A.*, 164:192, 1938.

[73] A. von der Heydt, S. Grossmann, and D. Lohse. Response maxima in modulated turbulence. *Phys. Rev. E.*, 67:046308, 2003.

[74] G. M. Wang, E. M. Sevick, E. Mittag, D. J. Searles, and D. J. Evans. Experimental demonstration of the violations of the second law of thermodynamics for small systems and short time scales. *Phys. Rev. Lett.*, 89:050601, 2002.

[75] H. Xu, M. Bourgoin, N. T. Ouellette, and E. Bodenschatz. High order lagrangian velocity statistics in turbulence. *Phys. Rev. Lett.*, 96:024503, 2006.

[76] H. Xu, N. T. Ouellette, and E. Bodenschatz. Multifractal dimension of lagrangian turbulence. *Phys. Rev. Lett.*, 96:114503, 2006.

[77] P. K. Yeung. Lagrangian investigations of turbulence. *Annu. Rev. Fluid Mech.*, 34:115, 2002.

[78] G. Zocchi, P. Tabeling, J. Maurer, and H. Willaime. Measurement of the scaling of the dissipation at high reynolds numbers. *Phys. Rev. E.*, 50:3693, 1994.